NASA Technical Memorandum 100130

Low Reynolds Number Nozzle Flow Study

Margaret V. Whalen
Lewis Research Center
Cleveland, Ohio

July 1987

NASA

LOW REYNOLDS NUMBER NOZZLE FLOW STUDY

Margaret V. Whalen
National Aeronautics and Space Administration
Lewis Research Center
Cleveland, Ohio 44135

SUMMARY

An experimental study of low Reynolds number nozzle flow was performed. A brief comparison was made between some of the experimental performance data and performance predicted by a viscous flow code. The performance of 15°, 20°, and 25° conical nozzles, bell nozzles, and trumpet nozzles was evaluated with unheated nitrogen and hydrogen. The numerical analysis was applied to the conical nozzles only, using an existing viscous flow code that was based on a slender-channel approximation. Although the trumpet and 25° conical nozzles had slightly better performance at lower Reynolds numbers, it is unclear which nozzle is superior as all fell within the experimental error band. The numerical results were found to agree with experimental results for nitrogen and for some of the hydrogen data. Some code modification is recommended to improve confidence in the performance prediction.

INTRODUCTION

Electrothermal thrusters, such as arcjets and resistojets, have the potential for high performance. These thrusters operate at high temperature and low thrust levels, which result in low Reynolds number nozzle flow. In the low Reynolds number regime, the flow boundary layer occupies a large portion of the flow area. These thick boundary layers can result in reduced thruster performance because of increased viscous losses. It is felt that through proper selection of the nozzle geometry these losses could be minimized.

In the past, work has been done in the low Reynolds number regime for supersonic nozzles (refs. 1 and 2), for chemical laser nozzles (refs. 3 to 5), and for low-density hypersonic nozzles (refs. 6 and 7). General consensus from these studies was that the viscous boundary layers in the nozzles were very large and that the flow could become fully viscous, with no inviscid core, as the Reynolds number was decreased. Rothe (ref. 1), in his electron-beam studies, showed that in supersonic nozzles, at a Reynolds number of 500, a small inviscid core exists in the flow and that below a Reynolds number of 300 the flow was fully viscous with no indication of an inviscid core. Driscoll (ref. 3) conducted a boundary-layer study in chemical laser nozzles and found that for axisymmetric nozzles the flow becomes fully viscous below a Reynolds number of about 1000. Whitfield (ref. 6) performed an investigation involving hypersonic nozzles and found that the boundary layer occupied as much as 80 percent of the nozzle exit area. These thick boundary layers contributed to the viscous losses in the nozzles by displacing the inviscid core, so that in the divergent section, the core density was increased and the velocity was decreased.

Early work in the area of nozzle performance has generally dealt with conical nozzles of varying half angles and area ratios. Murch, et al. (ref. 8),

examined 10°, 20°, and 30° conical nozzles and also tested bell and horn nozzles. The tests were performed with heated hydrogen and nitrogen for Reynolds numbers ranging from 400 to 4000. The results showed performance losses of up to 30 percent at low Reynolds numbers. A more recent study by Brophy, et al. (ref. 9), compared a modified bell and a 19° conical nozzle for arcjets. Recently, Grisnik, et al. (ref. 10), investigated the flow through four different nozzle contours. This study was performed with unheated hydrogen and nitrogen, and indicated that within experimental error the four contours had essentially the same performance.

Studies by Edwards and Jansson (refs. 11 to 13) investigated the loss mechanisms of a resistojet. Boundary-layer effects on nozzle performance and the importance of operating Reynolds number in the design of resistojet nozzles were discussed. Concerns have also been raised about difficulties in measuring the performance of thrusters in vacuum environments. Yoshida, et al. (ref. 14), showed that the ambient pressure of the vacuum chamber has a significant effect on performance measurements. Recently, Manzella, et al. (ref. 15) found that the effects on performance measurements occurred when testing with hot gases and suggested that these effects were due to convective heat transfer losses. The study presented herein used unheated gas flow to eliminate this loss mechanism. Another study by Sovey, et al. (ref. 16), showed that the ratio between the nozzle inlet pressure and the ambient pressure in the vacuum chamber needed to be lower than 10^{-3} to assure that a shock was not present in the nozzle and thus affecting performance of the nozzle. This consideration becomes particularly important for measurements at higher flowrates.

Several studies have examined the transonic region of supersonic nozzles. Back, et al. (refs. 17 and 18), investigated the influence of the contraction section of conical nozzles. Moreover, they measured and predicted flows. The performance was found to be relatively insensitive to the nature of the flow in the convergent section, but the radius of curvature through the throat region did affect the discharge coefficient. Work by Campbell and Farley (ref. 19) on converging-diverging nozzles indicated that a decrease in the divergent half angle resulted in increased thrust. Further, Back and Cuffel (ref. 20), found that for a relatively high Reynolds number flow, (10^6), the mass flow through the throat was affected by the throat configuration. The discharge coefficient was shown to decrease for a decrease in the ratio of throat radius of curvature to throat radius. This was corroborated by Cuffel, et al. (ref. 21), and again the convergent half angle was found to have little influence on discharge coefficient. Hopkins and Hill (ref. 22) developed a method to numerically predict the flowfield in the transonic region of nozzles. It was shown that the most significant geometric factor influencing flow through the throat was the radius of curvature. Apparently, the shape and location of the sonic line was altered by the curvature of the throat, and the effect of the convergent angle was found to be secondary, unless the radius of curvature was less than the throat radius. Kuluva and Hosack (ref. 23) examined the discharge coefficient in low Reynolds number flow. Their work indicated that velocity slip at the wall was significant at Reynolds numbers below 10^3 and that the throat curvature became important at Reynolds numbers below 200. Milligan (ref. 24), also indicated that slip velocity at the nozzle wall should be taken into account.

Rae (refs. 2 and 25) developed a numerical code which used a slender-channel approximation to predict viscous effects and the performance of

low-density nozzle flows. Rae's method used equations for the slender-channel approximation developed by Williams (ref. 26). The latter was an analytical study which involved compressible flows in convergent-divergent channels and yielded results regarding viscous effects, pressure ratio at the throat and discharge coefficient. Rae used the slender-channel approximation in conjunction with slip boundary conditions to predict nozzle performance in most of the Reynolds number range appropriate for electrothermal thrust devices. However, this technique was only capable of obtaining solutions for certain combinations of Reynolds number, wall angle, wall temperatures, and gas properties. The envelope of conditions for the successful use of this code was not fully defined. Results obtained from the code have been compared to Navier-Stokes solutions by Mitra and Fiebig (ref. 27). These solutions showed differences originating at the throat, but the solutions converged farther downstream.

The work presented here includes an experimental study of low Reynolds number nozzles and a brief comparison of some of the experimental performance data to numerical performance predictions using the slender-channel approximation. In attempting to improve the performance of electrothermal thrusters, the evaluation of the performance of various nozzle contours was considered to be significant. Nozzle performance is affected by many factors including nozzle contour, area ratio, and operating temperature. In the experimental portion of this investigation, several different nozzle contours were selected for performance evaluation with unheated gas flow. It was felt that loss mechanisms could be better quantified and identified using unheated gases.

The series of experiments compared the performance of conical nozzles with 15°, 20°, and 25° half angles, bell nozzles and trumpet-shaped nozzles. Data with unheated nitrogen and hydrogen were taken for each nozzle. The nitrogen data included Reynolds numbers up to 6000 and hydrogen data were for Reynolds numbers up to 3500. The variation of specific impulse efficiency and discharge coefficient for each nozzle as a function of Reynolds number was evaluated for different area ratios and nozzle contours.

In addition to the experimental study, a numerical analysis of the conical nozzles was undertaken. This analysis used an existing code developed by Rae, discussed previously. The code was run in an attempt to determine whether the slender-channel approximation was valid for conical nozzle designs and flow conditions considered here.

NOMENCLATURE

A_{code}	flowrate generated by the viscous flow code
A_{given}	flowrate based on experimental data
B	Reynolds numbers based on reservoir conditions
C_T	thrust coefficient
M*	throat Mach number at centerline of nozzle
M_e	nozzle exit Mach number at centerline of nozzle
Re	Reynolds number based on throat conditions

r/r^*	ratio of throat radius of curvature to throat radius
X_{max}	axial location of nozzle exit normalized to throat radius
X_0	axial location of convergent section normalized to throat radius
ϵ	area ratio
θ_1	convergent half angle of nozzle
θ_2	divergent half angle of nozzle

APPARATUS AND PROCEDURE

Experimental Apparatus

The facility used for the nozzle testing was a 0.91 m (3.0 ft) diameter by 1.82 m (6.0 ft) long vacuum tank. A 30 cm pipe connected the tank to a blower with a rated performance of 1×10^5 liter/min (3900 ft^3/min (cfm)), run in series with a roughing pump with a rated performance of 2×10^4 liter/min (760 cfm). The facility was capable of pressures as low as mid-10^{-4} torr. Typical tank pressures with flowing gas varied from 6×10^{-3} to 0.2 torr, depending on gas type and mass flowrate. The tank pressure was measured using a cold cathode ionization gauge, which had errors of up to ±20 percent in the low pressure range (10^{-3} torr). Tank pressures less than 10^{-2} torr were obtained in the tests with Reynolds numbers less than 2000. These tank or background pressure readings were used to correct all the measured thrust readings, and to determine the pressure ratio between the inlet pressure and this background pressure. As mentioned above, a previous study (ref. 16) determined that this pressure ratio must be lower than 10^{-3} torr in order to assure that a normal shock did not appear in the nozzle.

The mass flowrate measurements used laminar flow, heated wire type flowmeters. For these flowmeters, the gas flow was proportional to wire input current, for a constant wire temperature. Two flowmeters, covering the ranges from 0 to 5 standard liters/min (slpm) and from 0 to 50 slpm, were used in these tests. The flowmeter was factory calibrated for hydrogen. The nitrogen values were obtained by using the manufacturer-supplied correction factor. The error in the flow measurement in the 0 to 5 slpm flowmeter was less than 1 percent over the entire range. The flow measurement error of the 0 to 50 slpm flowmeter was from 3 to 5 percent over the test range (6 to 26 slpm).

The thrust measurements were obtained using a flexure-type thrust stand, capable of measuring forces as low as 2.2 mN (0.5 mlb). A schematic diagram of the thrust stand is shown in figure 1. The thrust stand consisted of a horizontal mounting plate supported by two sets of four flexure plates. This arrangement allowed motion in the horizontal direction. The design of the flexures resulted in a large displacement for a small force. This design also reduced thermal and vibrational problems. The thermal expansion of the thrust stand components, when running hot flow tests, was negligibly small compared to the thrust stand displacement. Any high-frequency vibrations were prevented from reaching the thruster mounting plate due to the low resonant frequency of the flexures. A magnetic damper assembly was used to remove the low-frequency vibrations. The damper consisted of a permanent magnet attached to the

thruster mounting plate, and inserted into an annular electromagnet. The output of the electromagnet was dependent upon the movement of the thruster mounting plate. The movement of the thruster plate was detected by a linear variable displacement transducer (LVDT). The signal from the LVDT was sent to a chart recorder, which recorded the displacement. The LVDT output was also amplified and used to energize the electromagnet of the damper assembly. The magnetic field produced in this way then applied a force on the permanent magnet opposing the motion of the thrust plate.

The thrust range of the thrust stand could be varied by changing the stiffness of the flexures or the stiffness of the propellant feed tube, which was designed to also be a flexure. The feed line was 0.318 cm (0.125 in.) thin wall stainless steel tubing which was connected perpendicularly to the axis of motion of the thrust stand, and thus acted as an additional flexure.

Calibration was performed by adding known weights to a pulley assembly and deflecting the thrust stand a given amount. The calibration was recorded on a chart recorder. The variability in thrust stand movement was small and reproducible. The thrust stand measurement variability was less than 5 percent at low thrust values and less than 2 percent at higher thrust levels, based on these calibrations.

The effect of circulating gases in the vacuum chamber was determined by flowing gas through an orifice mounted close to the stand and checking for deflection of the thrust stand. The deflection ranged from 2.2 to 8.9 mN (0.5 to 2 mlb) depending on flowrate. The influence of circulating gases was negligible after installing a wind shield between the nozzle exit and thrust stand.

The nozzles, designed to be interchangeable, were clamped to an assembly mounted on the thruster mounting plate. The assembly consisted of a 1.27 cm (0.5 in.) o.d. aluminum tube with stagnation pressure and temperature taps, feed line attachment and a flange which mated to the flange on each nozzle. The nozzles were clamped to this assembly as shown in figure 2. The gas inlet pressure was measured using a stainless steel, diaphragm type transducer. The range of the pressure transducer was from 0 to 2.4×10^5 N/m^2 (0 to 20 psia). The pressure tap was a 0.159 cm (0.0625 in.) tube located approximately 5.08 cm (2 in.) upstream of the nozzle throat. The pressure reading calibration was checked before each test and the error was found to be less than 1 percent of full scale. The gas temperature was measured using a stagnation type probe with a chromel-alumel thermocouple mounted in the gas stream about 5.08 cm (2 in.) upstream of the nozzle throat. Temperature measurement errors were estimated to be ±2 °C.

Five sets of converging-diverging nozzles were designed for this study. Each set of nozzles had a different diverging contour with area ratios (exit area/throat area) of 25, 50, 100, 150, and 200. Each of the nozzles was machined from stainless steel and had a flange piece electron beam welded to it. The converging section was the same for each nozzle. It had an o.d. of 1.27 cm (0.50 in.), an i.d. of 0.94 cm (0.37 in.), and converged at a 45° angle to a 0.152 cm (0.060 in.) throat diameter.

Three sets of conical nozzles were machined with 15°, 20°, and 25° half angles in the diverging section. Figure 3 provides an indication of the range of sizes of the 20° conical nozzles. The 15° and 25° nozzles are similar, with slightly different diverging section length. A 15° conical nozzle with an area ratio of 25:1 was not available for testing. The design drawing of these nozzles is shown in figure 4, with the dimensions and area ratios. The throat section of these nozzles was a cylindrical section, 0.152 cm (0.060 in.) in length, with the radius of the converging and diverging sections machined so there was no corner or step.

The fourth set of nozzles had a diverging section with a bell contour. The set of bell shaped nozzles is shown in figure 5. These nozzles were designed using a technique developed by Rao (ref. 29). This technique assumed isentropic flow and used a variational method to design the wall contour. The method of characteristics was used to construct the nozzle contour for given flow conditions. The computer code used to develop the different bell contours required area ratio, radius of curvature into and out of the throat, and the flow conditions. The result was coordinates that were used to plot the nozzle contour. The coordinates were subsequently supplied to a computer controlled lathe which machined the nozzles. Figure 6 shows the basic design of the bell nozzles as well as nozzle dimensions and area ratios.

The final set of nozzles designed had trumpet shaped diverging contour sections. Figure 7 depicts the trumpet nozzle size variation with area ratio. This contour was designed as shown in figure 8. A circular arc was drawn starting from the throat and extending out to the diameter necessary for the different area ratios. These nozzles were also machined by using a computer controlled lathe. The dimensions and area ratios are listed in figure 8.

Experimental Procedure

Testing of the nozzles involved consideration of four parameters: the nozzle contour, the nozzle area ratio, the gas type, and the Reynolds number. A total of 24 nozzles was tested. The nozzles with 15° half angle diverging sections had area ratios of 50:1, 100:1, 150:1, and 200:1. The 20° and 25° half angle conical nozzles, the bell contour nozzles and the trumpet shaped nozzles consisted of five nozzles each with area ratios of 25:1, 50:1, 100:1, 150:1, and 200:1. Testing was done with two gases, hydrogen and nitrogen. The Reynolds number was based on throat conditions and was equal to four times the mass flowrate divided by pi, the viscosity and the throat diameter. The Reynolds number was varied by changing the mass flowrate. The range of Reynolds numbers tested was from 150 to 3500 for hydrogen, and from 500 to 6000 for nitrogen. Two ranges of thrust were required to cover this range of Reynolds numbers: 3.0 to 25.3 mN (0.7 to 5.7 mlb) and 12.0 to 91.7 mN (2.7 to 20.6 mlb).

Prior to testing, the flexures on the thrust stand were adjusted to accommodate the selected thrust range. The nozzle was then clamped in place on the thruster assembly (see fig. 2), the nozzle exit was plugged, and the assembly was pressure leak checked. If the gas pressure did not drop in approximately 1 min, the system was considered leak tight. After the leak test, the thrust stand assembly was put into the tank and the tank was sealed and evacuated. The gas feed system was also evacuated and purged several times to assure that the system was clean and only contained the test gas. When the tank pressure

stabilized, the thrust stand was calibrated. The calibration was performed at least twice prior to the recording of any thrust measurements to assure reproducibility, and to allow adjustment of the zero point if necessary. A mass flowrate was then set and the thrust zero checked before and after each thrust measurement. The thrust measurement was recorded twice for each flowrate (or Reynolds number). Data were taken for hydrogen flowrates from 1 to 26 slpm and for nitrogen flowrates from 0.5 to 6 slpm. This procedure was followed for all nozzles, with both gases and over both thrust ranges. In all tests, the gas was at ambient temperature.

The following data were collected for each test point: flowrate, inlet gas temperature, gas total pressure at the nozzle inlet, the thrust reading, and tank pressure. These values, along with gas type, thrust calibration, the nozzle throat and exit diameter, and the number of data points were input to a data reduction program.

The data reduction program converted all the input values into SI units and calculated the pressure ratio, thrust, specific impulse, thrust coefficient, Reynolds number, discharge coefficient, and nozzle specific impulse efficiency. The basic equations used in the data reduction are included in appendix A.

RESULTS AND DISCUSSION

An evaluation of the performance differences of several nozzle contours was undertaken in this investigation. The nozzles under consideration were for low thrust electrothermal devices which operate in the low Reynolds number range. In this flow regime, the major loss mechanism is due to viscous effects which are associated with the boundary layer of the flow. Most of the past studies were performed with a heated gas flow, which made it difficult to evaluate the loss mechanisms. Therefore, in an attempt to better understand these mechanisms, gases at ambient temperature were used. Thus, the heat transfer loss mechanism due to hot gas flow was eliminated.

The experimental portion of this study evaluated the performance of nozzles with conical, bell, and trumpet diverging contours. The parameters of importance in the study of unheated flow include the specific impulse, the specific impulse efficiency, the discharge coefficient, and the thrust coefficient. The specific impulse efficiency, specific impulse, and thrust coefficient are performance type parameters which gave similar results in nozzle performance trends; therefore, only the results of one of these parameters was included. The experimental results included were specific impulse efficiency, and discharge coefficient variations with Reynolds number.

The numerical analysis was used only to evaluate the conical nozzles because of the limitations of the numerical code. In essence, this code was run to determine where the slender-channel approximation was valid for the nozzles considered and also to compare the predicted results with the experimentally measured performance.

Experimental Results

Four variables were involved in the nozzle testing; therefore, the approach to the data presentation had to take all four variables into consideration. The data presented considers each gas separately over a range of Reynolds numbers. The Reynolds number range for nitrogen was from 500 to 6000 and the range for hydrogen was from 150 to 3500. The data was plotted to determine the performance variation for each contour and for each area ratio. Several loss mechanisms were considered in the study, including losses due to incomplete expansion, viscous losses, and divergence losses.

The specific impulse (I_{sp}) efficiency is defined as the ratio of actual specific impulse to the theoretical maximum I_{sp}. This efficiency indicates the nozzle losses due to viscous and divergence losses. The theoretical maximum specific impulse of nitrogen and hydrogen at room temperature are 80 and 300 sec, respectively. The data obtained for I_{sp} efficiency was plotted for each each nozzle contour in order to observe the effect of area ratio. It was also plotted for each area ratio in order to compare the variation due to contour differences. Each I_{sp} efficiency plot also shows the effect of increasing Reynolds number.

The I_{sp} efficiency for different area ratio conical, bell, and trumpet nozzles run on nitrogen are shown in figures 9(a) to (e). As can be seen, the I_{sp} efficiency decreases with decreasing Reynolds numbers for all the nozzles. The maximum difference in efficiency for the different area ratio 15° conical nozzles was 3 percent at the lowest Reynolds number and 2 percent over the rest of the range as shown in figure 9(a). The 20° conical nozzles, figure 9(b), had a 2 percent variation in the I_{sp} efficiency over the entire Reynolds number range. The data for both the 15° and 20° conical nozzles were within expected experimental error; therefore, no area ratio could be considered significantly better than another. However, for the 25° conical nozzles, there does appear to be some difference in the performance for different area ratios. As the Reynolds number increased, the efficiency of the nozzle with an area ratio of 25:1 did not increase to the same level as the other 25° nozzles, figure 9(c). Its efficiency was about 3 percent lower than the other nozzles at the higher Reynolds numbers. The efficiency of the conical nozzles were all within 5 percent of each other over the entire Reynolds number range. Although differences were noted for these nozzles, the differences were within experimental error for the low Reynolds number cases, and just outside experimental error for the higher Reynolds number cases. The error bars on figure 9(a) indicate this.

The efficiencies of the bell contour nozzles ranged from 72 to 87 percent as shown in figure 9(d). At the lower Reynolds numbers, the nozzles with an area ratio of 50:1 had slightly higher efficiency. The data showed higher differences at the low Reynolds numbers and area ratio appeared to have little effect as the Reynolds numbers was increased.

For the trumpet nozzles, the efficiency differences were about 4 percent below a Reynolds number of 2000, and about 3 percent at higher Reynolds numbers. The 25:1 area ratio nozzle had the lowest efficiency over the entire Reynolds number range. Again, at low and high Reynolds numbers the differences due to area ratio were within experimental error.

When the data for hydrogen was presented in the same fashion, the efficiency trends were similar for each group of nozzles. However, the effect of area ratio was more pronounced compared to the nitrogen data, as seen in figures 10(a) to (e). For the conical nozzles, with half-angles of 15°, 20°, and 25°, figures 10(a) to (c), respectively, as the Reynolds number increased above about 1500, differences in efficiency with area ratio were apparent. The efficiency increased with increasing area ratio; the efficiencies of the 200:1 area ratio nozzles were approximately 4 percent higher than those of the 25:1 nozzles for both the 20° and 25° conical nozzles, and 3 percent higher than the 15° conical nozzles with a 50:1 area ratio. The efficiency increased about 1 percent with each increase in area ratio. Data presented by Murch (ref. 8) for 20° conical nozzles run with hydrogen at 815 °C (1500 °F) showed the opposite trend of efficiency with area ratio. The percent differences in the Murch data were not discussed making it difficult to determine whether this 1 percent difference fell within experimental error. The efficiency was found to increase with decreasing area ratios ranging from 20:1 to 200:1. The losses due to viscous flow can be increased due to heat transfer at the nozzle wall, and these losses would be expected to increase with higher area ratio and therefore, longer nozzles. However, because of the experimental error in the data presented here, and the unknown value of the experimental error in the Murch data, it is possible that the data are consistent.

The bell nozzles tested with hydrogen had efficiencies generally lower than the conical nozzles discussed above. However, the efficiency generally increased with Reynolds number at lower area ratios (fig. 10(d)). The nozzle with the 25:1 area ratio had the highest efficiency over the range of Reynolds numbers tested. The differences in the efficiency with area ratio tended to decrease with increasing Reynolds number. This trend was expected because these nozzles were designed assuming isentropic flow. The efficiency is expected to peak at higher Reynolds number than tested in this study, and the efficiency of the bell contoured nozzles at higher Reynolds number may be larger than any of the other nozzles considered here because as Reynolds number increases the conditions can approach isentropic flow.

The trumpet nozzles had efficiencies in the same range as those of the conical nozzles, with the efficiencies in the Reynolds number range below 2000 slightly higher than the efficiencies of the conical nozzles, as shown in figure 10(e). The trumpet nozzle efficiencies only increased slightly at Reynolds numbers above 2000. The larger area ratio nozzles were generally higher in efficiency over the Reynolds number range for hydrogen.

Figures 11(a) to (e) show the efficiency differences of the contours at each area ratio for the tests run with nitrogen. For Reynolds numbers below 2000, the bell nozzles had the lowest efficiency of all the area ratios tested. Figure 11(a) shows the efficiencies for the 25:1 area ratio nozzles. Below a Reynolds number of 2000, the efficiencies of the 25:1 conical and trumpet nozzles were within experimental error of each other. The efficiency of the bell nozzle was lower and dropped to 5 percent below the other contours at a Reynolds number of 500. The 15° and 20° conical nozzles had efficiencies 2 to 4 percent higher at Reynolds numbers above 2000 for area ratios of 50:1 and 25:1, respectively. For area ratios of 100:1 and greater, shown in figures 11(c) to (e), all the data was within 3 percent at Reynolds numbers above 2000. The only trend among these different higher area ratios was that the efficiency of the bell nozzles was lower for each. Also, the bell efficiency was still increasing while the other efficiencies remained constant.

This was expected because of the design technique used for the bell nozzles. That is, at higher flowrates the flow is more isentropic. At lower Reynolds numbers the trumpet nozzles generally gave higher efficiencies than those of the other contours.

Data for the various nozzles operated on hydrogen are shown in figures 12(a) to (e). The data for area ratios of 25:1 and 50:1, presented in figures 12(a) and (b), display little difference between the performance of the different contours. At Reynolds numbers below about 1000, as the area ratio was increased, figures 12(c) to (e), the 25° conical and trumpet nozzles performed slightly better than the other nozzles. There was likely some trade-off between the divergence losses in these more rapidly expanding nozzles and the viscous losses along the nozzle wall, as the area ratio was increased.

The efficiency of the bell nozzles in the low Reynolds number range was lower than the other nozzles and dropped with increasing area ratio. The bell nozzle designs were not optimized to include boundary layer effects, as is done with larger thrust chemical propulsion nozzles where the boundary layer is known to be thin. In these low Reynolds number nozzles, the flow was viscous with a thick boundary layer and, as found in studies by Rothe (ref. 1), may become fully viscous with no indication of any inviscid core for Reynolds number less than 300. It was decided that optimization of the bell design for boundary layer effects was not practical for flows with thick boundary layers or for fully viscous flows. The comparison between different nozzle contours was on the basis of geometrically similar area ratios, which had differences of 4 percent or less at the same area ratio.

Generally, the efficiencies of the nozzles using either nitrogen or hydrogen were within experimental error of each other. The error was 5 percent for nitrogen data below Reynolds numbers of 2000 and for hydrogen data below Reynolds numbers of 1000. At higher Reynolds numbers, the error was 2 percent for both gases. The trends in both sets of data were similar. The bell nozzles as designed were lower in efficiency, except for the 25:1 area ratio, which was within the scatter of the other data. Efficiency of bell nozzles would change if the boundary layer was taken into account, as was done in an investigation by Brophy, et al. (ref. 9), on arcjet nozzles. The trumpet nozzle efficiency appeared to be better for Reynolds numbers below 2000, particularly at higher area ratios. However, given the range of the accuracy of the thrust stand, it appears that there was little difference between the nozzle configurations. The efficiencies of the 25° conical nozzles were generally within 1 to 2 percent of the efficiencies of the trumpet nozzles. This is well within experimental error. It should be further noted that the conical nozzles have the advantage that they are typically simpler to fabricate.

The data presented by Murch (ref. 8) for tests with hydrogen showed that as Reynolds number increased, the bell and the 20° conical nozzles with area ratios of 100:1 were within 1 percent of each other, with the bell being the larger. The data for the trumpet nozzles showed that its efficiency was about 1 percent above that of the bell and conical shapes for Reynolds numbers of between 400 and 1200. Murch did not include design details or detailed test procedures; therefore, the comparison can only be made on a relative basis. The trends exhibited were similar, although the efficiency values were different.

Recently Grisnik, et. al. (ref. 11), reported results of a study in which unheated nitrogen and hydrogen were used to test a 20° conical, a bell, a trumpet, and a modified trumpet nozzle. This data showed all of the nozzles tested had the same performance to within experimental error, which was 5 percent in that study. It should be noted that nozzles compared by Grisnik had area ratios ranging from 120:1 and to 150:1. The nozzle efficiency ranges obtained for the hydrogen data were similar to the data obtained in this study. The nitrogen data reported was 3 to 4 percent higher than the data obtained in this study at Reynolds numbers below 2000, but the trends shown were similar.

The discharge coefficient was the other parameter selected for study in this experimental investigation. The discharge coefficient is defined as the ratio of the measured mass flowrate to the theoretical maximum mass flowrate through a nozzle assuming isentropic flow. The discharge coefficient indicated the mass losses due to viscous effects in the nozzle throat. The discharge coefficient data was presented in the same format as the specific impulse efficiency data with variation of contour and area ratio presented as a function of Reynolds number.

The nitrogen discharge coefficient data for the different nozzle contours are presented in figures 13(a) to (e). Results for the 15°, 20°, and 25° conical nozzles are shown in figures 13(a) to (c). As can be seen, the flow coefficient decreased with decreasing Reynolds number. This trend was expected because at lower Reynolds numbers the boundary layer extends across more of the throat and, thus, more of the mass flows through the viscous layer. As the Reynolds number increased, the discharge coefficient rose to a constant value and showed no difference between area ratios, which was also expected.

The discharge coefficient data for the five bell contoured nozzles is presented in figure 13(d). The discharge coefficients are again seen to be the same within the error of the flow measurement at the higher Reynolds numbers. At low Reynolds numbers, the discharge coefficient dropped as expected, except for the nozzle with the 25:1 area ratio. It is suspected that differences in the throat curvature may have accounted for this performance difference, but the bell nozzles all have the same inlet throat radius of curvature and the same, although different from the inlet, outlet curvature. Another possibility for discharge coefficient not behaving as expected may be surface roughness effects in the throat region. However, surface roughness was expected to have a negligible effect with the thick boundary layers occurring at these low Reynolds numbers.

The trumpet nozzle data for discharge coefficient is presented in figure 13(e). The trumpet nozzle discharge coefficients were lower than the other contours, at low Reynolds numbers and the percent difference was about 4 percent at the higher Reynolds numbers. The lower discharge coefficient was an indication that the throat boundary layer in the trumpet nozzles was larger, thus, the viscous losses in the throat region were higher.

The discharge coefficient data for the different nozzle contours run with hydrogen is presented in figures 14(a) to (e). The data in figures 14(a) to (c) showed the same trends as the discharge coefficient data of the 15°, 20°, and 25° conical nozzles tested with nitrogen. However, as the Reynolds numbers increased, the discharge coefficient values did not increase to the same level as those for the nitrogen data. For Reynolds numbers higher than 600, the flowrate data was obtained using the flowmeter with a range of 0 to

50 slpm described in the Experimental Apparatus section. This flowmeter was found to consistently read 3 to 5 percent low over the range used (6 to 26 slpm). Since the discharge coefficient is a ratio involving the actual mass flowrate, it follows that the values obtained would likewise be expected to be 3 to 5 percent low. Correction of the data by 3 to 5 percent for Reynolds numbers from 600 to 3600 would raise the level of values up to the same range as obtained in the nitrogen tests. The nitrogen data spanned a flowrate range of 0.5 to 6 slpm, and used a flowmeter with an error of less than 1 percent.

Figure 14(d) shows the discharge coefficients of the bell contour nozzles. Again, the data followed the expected pattern except for the 25:1 area ratio nozzle. It was not clear why this discrepancy occurred. The data above a Reynolds number of 600 should be corrected upward by 3 to 5 percent as a result of error in the flow measurement.

At increasing Reynolds numbers the discharge coefficients are less distributed and appear to approach some limiting value. The trumpet nozzle discharge coefficient data for hydrogen, shown in figure 14(e), was lower over the entire range of Reynolds numbers than the other nozzles. Correction of the measured flowrate would, again, raise the data for Reynolds numbers above 600 to the values obtained with nitrogen. The implication again was that for the lower Reynolds numbers the viscous losses in the throat region were greater than those of the other contours.

Figures 15(a) to 15(e) are plots of the discharge coefficients for nitrogen for different nozzle contours at each area ratio. At lower area ratios of 25:1 and 50:1, shown in figures 15(a) and (b), respectively, the trumpet nozzles had lower discharge coefficients. As the area ratio increased, the trumpet nozzles had lower discharge coefficients in the low Reynolds number range, as shown in figures 15(c) to (e) for area ratios of 100:1, 150:1, and 200:1, respectively. The discharge coefficients of the bell nozzles also tended to decrease with increasing area ratio for the lower Reynolds numbers. At larger Reynolds numbers, the 15°, 20°, and 25° conical nozzles had essentially the same discharge coefficients. When this data was plotted for hydrogen, the same general trends were exhibited, as shown in figures 16(a) to (e) for area ratios of 25:1, 50:1, 100:1, 150:1, and 200:1, respectively. The variations in discharge coefficient were attributed to differences in boundary layer thickness in the throat region, and viscous losses associated with the boundary layer.

Several ideas were explored as a means of explaining the variation in discharge coefficient results, among the possible factors was the influence of geometry in the throat region. The geometry of the throat region included the converging section, the throat radius of curvature, and the surface condition of the nozzle wall. As mentioned earlier, the inlet side or convergent section of each of the various nozzle contours was the same. The convergent angle was 45° in each nozzle and the measured throat diameters were all within 2 percent of each other. Accordingly, the inlet geometry of the different nozzles was not considered to be a factor in the variation of the discharge coefficients. In addition, previous experimental and numerical studies, have indicated that the convergent nozzle contour does not affect the nozzle discharge coefficient (refs. 20 and 21).

Nozzle throat geometry begins to affect the flowfield at the point of tangency between the convergent angle and the circular radius at the throat. For

the nozzles tested, the radius of curvature was designed to be the same on the throat inlet side; however, the throat radius of curvature on the outlet side was different for each contour. For comparison each outlet radius of curvature was normalized to the throat radius. These ratios were 8 for the 15° conical nozzles, 6.7 for the 20° conical nozzles, 5.2 for the 25° conical nozzles, 1 for the bell nozzles, and 40 for the trumpet nozzles. The ratios for the conical nozzles had to be estimated because the actual radius was obtained by blending the throat and divergent section contours. This was done to simplify the fabrication of these nozzles, hence the actual value could not be determined. The trend in both the nitrogen and hydrogen tests was for increases in discharge coefficient to correspond to decreases in the outlet radius of curvature. Data presented by Back (ref. 18) indicated an opposite trend, i.e., discharge coefficient increased with increasing radius of curvature. However, two significant differences exist between these sets of data. The data presented here was obtained with nozzles that did not have a constant radius of curvature through the throat, and the data was obtained for low Reynolds number flows (<10 000). On the other hand, Back's data was for high Reynolds number flow through nozzles with a constant radius of curvature through the throat. These differences make it difficult to make valid comparisons, but they indicate that this may be an area for further study. An important point here was that despite the low discharge coefficients in the low Reynolds number region, the trumpet nozzles, at least at higher area ratios, appeared to have better I_{sp} efficiencies than the other nozzles. Apparently, the gains made in the divergent section of the trumpet nozzles overshadowed the viscous losses in the throat region. It was suspected that further study of the throat region may further improve the performance of these small nozzles. Through improved design of the throat, the trumpet design may obtain even better efficiencies.

The surface condition of the nozzle throat region after machining may possibly affect the discharge coefficient. However, this was not considered likely to be significant for the lower Reynolds number flows. In low Reynolds number flows, the boundary layer was thick, as indicated by Rothe (ref. 1) and others. Thus, the surface roughness of the wall in the throat region and downstream were not likely to have a significant effect on the flow field unless the surface roughness was on the order of the boundary layer thickness, as is possible in high Reynolds number flow. The effect of surface roughness should be verified in subsequent testing, but, as indicated above, is not expected to be significant in the low Reynolds number regime.

Numerical Results

A computer code for calculating viscous flow in nozzles was developed by Rae (ref. 25). The performance predictions given by this code were used for comparison with the experimentally measured performance. The method employed was based on the slender-channel approximation of the Navier-Stokes equations. The slender-channel equations are formally identical to the boundary layer equations. However, unlike boundary layer solution procedures, the axial pressure gradient is unknown and must be calculated as part of the solution. The equations are written in cylindrical coordinates for steady, axisymmetric flow. The basic equations and their nondimensional form are listed in appendix B. In the solution of the equations, the boundary conditions on the axis resulted in all radial derivatives vanishing. At the nozzle wall, rarefied flow boundary conditions were used, allowing a velocity slip and a temperature jump to exist. In this approach, Rae assumed the gas to obey the perfect-gas law, with

a viscosity that is proportional to a power of temperature. The Prandtl number and the specific-heat ratio were taken to be constant.

The numerical procedure began at a location upstream of the nozzle throat. For the cases considered here, this location was set at the beginning of the convergent section. The slender-channel equations were solved using an implicit finite difference scheme, which marched downstream through the nozzle. The required inputs to this code were: the reservoir conditions, nozzle geometry, gas properties, and, if heat transfer was included, the distribution of wall temperature. For the cases calculated in this study, the adiabatic wall boundary condition was used. This was considered a good approximation because the experimental tests selected for comparison were run with an unheated gas.

This program has an option that permits the user to input either a known mass flowrate or Reynolds number wherein the flowrate is calculated for the given nozzle geometry. All the cases run with nitrogen had the mass flowrate calculated as part of the solution. When tried with the known mass flowrate, some of the hydrogen and all of the nitrogen cases failed to converge to a solution. Therefore, for the data presented here only the nitrogen cases with calculated flowrates were included. The hydrogen cases included some with a known mass flowrate and some with code calculated mass flowrates.

The Rae code was written for nozzles with conical geometries; therefore, only conical nozzle performance could be compared. For this comparative study, the 15°, 20°, and 25° half angle conical nozzles with area ratios of 50 and 150 were selected. Data from these six nozzles at three different Reynolds numbers for both nitrogen and hydrogen were used as input to the code. In order to run the program, the nozzle geometry had to be defined with axial length normalized to the throat radius. The geometry included the half angle of the converging and diverging sections, the throat radius of curvature and definition of the axial length. These values are listed in table I for each nozzle considered. The throat of each nozzle was defined as the axial origin, the convergent section was then in the negative axial direction and the divergent section extended in the positive direction. The code was built on the assumption that the throat radius of curvature was constant; however, the conical nozzles were designed such that the radius of curvature on the inlet side of the throat was different from that on the outlet side. The inlet side of each nozzle had the same design; therefore, the inlet curvature was used. A complete list of input variables including their definitions is given in appendix C.

The numerical code developed by Rae (ref. 25) was used to generate performance predictions which were compared to the experimental performance data. The results obtained from the code for nitrogen and hydrogen are listed in tables II and III, respectively. The tables list the nozzles area ratio and half angle, the Reynolds number (B), the experimental flowrate (A code), the flowrate at which the code ran (A_{given}), the centerline Mach numbers at the throat and exit, and the thrust coefficient. For each nozzle and gas, three different Reynolds numbers flows were examined. In both the nitrogen and hydrogen cases, the highest Reynolds number case treated did not converge to a solution for any of the nozzles. For nitrogen, the Reynolds numbers were approximately 900, 3500, and 8900. The Reynolds numbers for hydrogen were about 550, 3750, and 6800. These Reynolds numbers have been redefined as required prior to input to the code.

The nitrogen cases listed in table II only ran to a solution when the code calculated the flowrate (A), and resulting flowrates were, with the exception of run number 20, lower than the experimentally measured values. The flowrates that were calculated are proportional to discharge coefficient and are related to Reynolds number (B). The Reynolds number input to the program was calculated as a function of nozzle inlet stagnation conditions (enthalpy, temperature, and pressure), and was not calculated the same way as the experimental Reynolds number. The latter was determined from the experimental mass flowrate and the throat conditions. Therefore, there was some mismatch or built-in error between the code required flowrate and Reynolds number. These values were not directly related as the experimental flowrate and Reynolds number were. This was believed to be the source of difficulty in running some of the cases with known flowrates. The code provided the option of calculating or inputting a known flowrate. The cases with N2 were all code generated flowrates.

For the hydrogen runs listed in table III, several cases were found to converge to solutions with the given flowrates. Apparently, an error was introduced into the Reynolds numbers and the flowrates for the other cases, similar to that of the nitrogen data. Therefore, these cases were run allowing the code to calculate the flowrate. Several cases for both gases were unable to converge to solutions with either the known or code calculated flowrate.

In Williams discussion of the slender-channel approximation (ref.26), the transport properties were assumed to vary as a power of temperature. Williams indicated that for a given wall angle and wall temperature, solutions were possible only for certain conditions of throat centerline Mach number, Reynolds number, ratio of specific heat and Prandtl number. Rae (ref. 2) also indicated that his code, which used this same approximation, had limitations and that there were concerns about accuracy. At low Reynolds numbers, it was probable that no solution with a supersonic core would be found. At high Reynolds numbers, accuracy could be reduced for two possible reasons: first, as the boundary layer thins, it would be described by fewer radial grid points, and second, the slip velocity decreases at the wall; thus, the integrals that are related to velocity would not be calculated correctly by Simpson's rule.

The cases that ran using the slender-channel approximation were compared to the experimental data. The performance parameter obtained from the code was thrust coefficient. The thrust coefficient indicates the increase in thrust due to expanding the gas through a nozzle as compared to thrust obtained if the chamber pressure acted only over the throat area.

The results obtained for the nitrogen cases are shown in table IV. The table gives the nozzle, the Reynolds number, the experimental and numerical thrust coefficient, and the percent difference between these values. The numerical results are for Reynolds numbers of 460 and 1850 (B of 900 and 3500), at area ratios of 50:1 and 150:1. The results showed that for 15° conical nozzle, the low Reynolds number point for the 50:1 nozzle was 7.6 percent higher than the experimental value, and the other numerical thrust coefficients were 3 to 3.5 percent higher. The results for the 20° conical nozzles showed the numerical results to be within 4 percent of the experimental thrust coefficients. The 25° conical nozzle results were within 3 percent of the experimentally obtained thrust coefficients.

The results obtained for hydrogen are shown in table V. Numerical results were obtained for Reynolds numbers of 260 and 1850 (B of 550 and 3750). In the hydrogen data, all the cases at a Reynolds number of 260 and the cases for the 15° cone with an area ratio of 150:1 and a Reynolds number of 1850 had code generated flowrates. In these cases, the percent difference between the experimentally and numerically obtained thrust coefficients ranged from 5 to 20 percent. Cases run with known flowrates showed differences of 3 percent or less. Kallis, et al. (ref. 29), used Rae's code to predict resistojet performance and also compared the predictions to experimental data. The code was run for a range of Reynolds numbers from 1000 to 7000. Differences between experimental and predicted performance ranged from 0 to 9.2 percent. The predictions obtained here were similar, except for the hydrogen cases with code generated flowrates.

The agreement between experimental thrust coefficients and computed thrust coefficients obtained from code generated flowrates for the two gases was very different. The nitrogen results agreed well, but the hydrogen agreement was poor in some cases. The poor results obtained for hydrogen were only for the low Reynolds number cases. It is suspected that the code was not accurate at modeling the Reynolds number range where most or all of the divergent section of the flow field was subsonic. As indicated earlier, Rae (ref. 25) had not accurately defined the limits of this code.

After running the code, it was found that there appeared to be a numerical stability problem related to the throat centerline Mach numbers. It was found that the program would terminate at centerline Mach numbers of 1.2 or higher. Other cases were unable to calculate the pressure gradient within the required number of iterations, and some cases could not get beyond the throat. The cases that did not run stopped for one of these reasons. It is believed that the higher Reynolds number cases that did not run could also have had geometry, Reynolds number or gas property conditions for which the slender-channel approximation was inappropriate.

An interesting result in the hydrogen numerical results was that the centerline Mach number at both the throat and exit were generally higher for the low Reynolds number case. The velocity profiles at several locations along the nozzle from the throat to the exit are compared in figures 17(a) and (b). The two cases presented are for the 15° conical nozzle with a 50:1 area ratio, at Reynolds numbers of 260 and 1850. At the throat, it is seen that the velocity profiles are approximately the same. But, at axial locations farther downstream, the velocity close to the centerline (ETA = 0 to 0.2) was significantly higher for the low Reynolds number case. This suggests that the higher centerline Mach number, especially at the exit, was to be expected.

Although the results predicted by Rae's code were reasonable in many cases, a word of caution is in order. As previously mentioned, the geometry written into this code and used in the cases presented here did not accurately describe the nozzles that were experimentally tested. Rae's code assumed a constant throat radius of curvature; however, the nozzles tested had different curvatures on the inlet and outlet sides of the throat. It is recommended that the geometric section of the code be refined to accommodate the variation of radius of curvature and to accommodate different contours. The addition of the throat curvature variation is also recommended because as previously discussed, some experimental studies have shown some differences in the discharge coefficient with changes in the throat radius of curvature.

CONCLUSIONS

The major goal of the study presented here was to evaluate and compare the performance of different nozzle contours. The study evaluated nozzles with different divergent section contours, including 15°, 20°, and 25° conical nozzles, bell nozzles, and trumpet nozzles. Area ratios of 25:1, 50:1, 100:1, 150:1, and 200:1 were tested for each nozzle, except for the 15° conical nozzle in which all of these area ratios were tested except the 25:1. The nozzles were tested with unheated nitrogen and hydrogen over Reynolds number ranges of 500 to 6000 and 150 to 3500, respectively.

The performance of the nozzles was generally within experimental error of each other over the Reynolds number range tested. The trends seen in the specific impulse efficiency were similar for both gases. The bell contour nozzles tended to be lower in efficiency than the other contours in the low Reynolds number range tested. At Reynolds numbers below about 2000, the trumpet and 25° conical nozzles performed slightly better than the other conical nozzles, and significantly better than the bell nozzles, for higher area ratios. But, these results were still within experimental error, which makes any recommendation quite difficult. The discharge coefficient results showed that the trumpet nozzles had the lowest values, particularly at the lower Reynolds numbers. This may indicate that the better performance of the trumpet nozzles may be further improved through a more careful design of the throat region. Reduction of the viscous losses at the throat could increase the overall performance of a nozzle.

Although the trumpet or 25° conical nozzles appeared to be slightly better designs, at lower Reynolds numbers, it is unclear which nozzle is better as all fell within experimental error. It is recommended that a similar comparison be made between these nozzles tested with hot flow to evaluate the effects of heat transfer on overall performance. The bell nozzle as designed is not recommended for use in low Reynolds number nozzles. Consideration should also be given to fabrication of these small nozzles. If performance differences are small, as indicated by these tests, and not a major driver in a particular application, the choice may be based instead, on which nozzle is easiest to fabricate.

The numerical results obtained using a computer code based on the slender-channel approximation, showed reasonable agreement with experimental results for nitrogen and for some of the hydrogen data. However, the code used did not correctly define the geometry of the nozzles tested. The code should be modified to more correctly define the nozzle geometry and therefore improve confidence in the performance prediction. The code was also found to have limited use in the Reynolds number range considered here, as no solutions were obtainable for the highest Reynolds numbers tried.

APPENDIX A - BASIC EQUATIONS FOR DATA REDUCTION

The measured thrust based on a momentum balance at the nozzle is

$$F_m = \dot{m}U_E + A_E(P_E - P_A) \tag{A1}$$

For the same flow conditions, the thrust in hard vacuum is

$$F_V = \dot{m}U_E + P_E A_E \tag{A2}$$

To account for the effect of the vacuum tank pressure in excess of hard vacuum, thrust is

$$F_A = F_m + P_A A_E \tag{A3}$$

Specific impulse was then obtained using F_A;

$$I_{sp} = \frac{F_A}{(\dot{m}\, g)} \tag{A4}$$

Thrust coefficient determined the increase in the thrust due to expanding the gas through a nozzle compared to thrust if the chamber pressure acted over the throat area only. It was calculated by;

$$C_T = \frac{F_A}{(P_c A^*)} \tag{A5}$$

The Reynolds number was calculated based on throat conditions and was

$$R = \frac{4\dot{m}}{(\pi\mu\, d)} \tag{A6}$$

The discharge coefficient indicated the mass flow losses due to viscous effects in the nozzle throat. It is the following ratio:

$$C_D = \frac{\dot{m}_A}{\dot{m}_I} \tag{A7}$$

The nozzle specific impulse efficiency is

$$N_{I_{sp}} = \frac{I_{sp,A}}{I_{sp,I}} \tag{A8}$$

LIST OF SYMBOLS

A_E	nozzle exit area, m^2
A^*	nozzle throat area, m^2
C_D	discharge coefficient
C_T	thrust coefficient
d	throat diameter, m
F_A	adjusted thrust, N
F_m	measured thrust, N
g	9.807 m/sec^2
I_{sp}	specific impulse, sec
I_{sp},A	measured specific impulse, sec
I_{sp},I	specific impulse assuming isentropic flow, sec
$\dot{m}$	mass flowrate, kg/sec
$\dot{m}_A$	measured mass flowrate, kg/sec
$\dot{m}_I$	theoretical maximum mass flowrate, kg/sec
$N_{I_{sp}}$	specific impulse efficiency
P_A	ambient (tank) pressure, N/m^2
P_c	inlet pressure, N/m^2
P_E	static pressure at exit plane of nozzle, N/m^2
R	Reynolds number
U_E	average nozzle exit velocity, m/sec
μ	viscosity, kg/(m sec)

APPENDIX B - BASIC EQUATIONS OF RAE'S CODE

For flow in slender-channels, the approximate equations of motion for steady axisymmetric flow in cylindrical coordinates are:

continuity,

$$\frac{\partial}{\partial Z}(\rho u) + \frac{\partial}{\partial r}(\rho v) + \frac{\rho v}{r} = 0 \tag{B1}$$

axial momentum,

$$\rho u \frac{\partial u}{\partial Z} + \rho v \frac{\partial u}{\partial r} = -\frac{dP}{dZ} + \frac{1}{r}\frac{\partial}{\partial r}\left(\mu r \frac{\partial u}{\partial r}\right) \tag{B2}$$

radial momentum,

$$\frac{\partial P}{\partial r} = 0 \tag{B3}$$

energy,

$$\rho u \frac{\partial h}{\partial Z} + \rho v \frac{\partial h}{\partial r} - u \frac{dP}{dZ} = \frac{1}{r}\frac{\partial}{\partial r}\left(\frac{r\mu}{Pr}\frac{\partial h}{\partial r}\right) + \mu\left(\frac{\partial u}{\partial r}\right)^2 \tag{B4}$$

The coordinates and the dependent variables are made dimensionless using throat radius and the reservoir conditions as:

$$x = \frac{Z}{r^*} \quad , \quad \sigma = \frac{r}{r^*}$$

$$U = \frac{u}{\sqrt{2H_o}} \quad , \quad V = \frac{v}{\sqrt{2H_o}}$$

$$P = \frac{p}{p_o} \quad , \quad D = \frac{\rho}{\rho_o} \quad , \quad \theta = \frac{h}{H_o}$$

In terms of these variables, the equations of motion become:

continuity,

$$P\frac{\partial}{\partial \eta}\left(\frac{\eta W}{\theta}\right) + \sigma_w \eta \frac{\partial}{\partial x}\left(\frac{PU}{\theta}\right) + 2\sigma_w' \frac{P\eta U}{\theta} = 0 \tag{B5}$$

momentum,

$$\frac{P}{\theta}\left(U\frac{\partial U}{\partial x} + \frac{W}{\sigma_w}\frac{\partial U}{\partial \eta}\right) = -\frac{\gamma - 1}{2\gamma}\frac{dP}{dx} + \frac{1}{Bn\sigma_w^2}\frac{\partial}{\partial \eta}\left(\eta\theta^{\omega}\frac{\partial U}{\partial \eta}\right) \tag{B6}$$

energy,

$$\frac{P}{\theta}\left(U\frac{\partial\theta}{\partial x}+\frac{W}{\sigma_w}\frac{\partial\theta}{\partial\eta}\right)=\frac{\gamma-1}{\gamma}U\frac{dP}{dx}+\frac{1}{B\eta\sigma_w^2}\frac{\partial}{\partial\eta}\left(\frac{\eta}{Pr}\sigma^{\omega}\frac{\partial\theta}{\partial\eta}\right)+\frac{2\theta^{\omega}}{B\sigma_w^2}\left(\frac{\partial U}{\partial\eta}\right)^2 \qquad (B7)$$

In these equations, density was eliminated by using the equation of state: $P = D\theta$. The radial velocity was transformed and appears at $W = V - U\eta\, d\sigma_\omega/dx$.

LIST OF SYMBOLS

B Reynolds number based on reservoir conditions

D ρ/ρ_0

H total enthalpy

h static enthalpy

P p/p_0

p pressure

Pr Prandtl number

r,z cylindrical coordinates

U,V $u/\sqrt{2H_0}$, $v/\sqrt{2U_0}$

u,v axial and radial velocity components

W $V - U\eta\, d\sigma_w/dx$

x,σ Z/r^*, r/r^*

γ specific heat ratio

η σ/σ_ω

θ h/H_0

μ viscosity

ρ density

σ_w r_w/r^*

ω exponent in viscosity and enthalpy relation

subscripts

o at reservoir conditions

w at wall

* at geometric throat

APPENDIX C - INPUT VARIABLES FOR VISCOUS FLOW CODE

A0	initial lower boundary of flowrate
A1	initial upper boundary of flowrate
ALPHT	temperature accommodation coefficient
ALPHU	velocity accommodation coefficient
ATEST	tolerance allowed for A
B	reservoir Reynolds number
DELX	initial delta X
GAMMA	specific heat ratio
OMEGA	temperature exponent in viscosity law
PR	Prandtl number
R1	throat radius of curvature normalized to throat radius
THETA1	half angle of convergent cone
THETA2	half angle of divergent cone
TW2	wall to temperature ratio (heat transfer case)
X0	initial X value (negative)
X1	begin reduced step size (throat region)
X2	restore original step size
XCUT	switch point for straight line extrapolation through saddle point
XIPG	defines method of calculating pressure gradient
XMAX	calculations stopped at this point
XPRINT	profiles printed at this interval
XTW1	used for heat transfer case
XTW2	used for heat transfer case
IBC	=1,heat transfer; =2,adiabatic wall
IETAPR	interval at which profiles printed
ISP	=0, print iterations; =1, print profiles only
MORE	if nonzero, more than one case will be run

NPRO if nonzero, profiles are not printed

NRUN run number

REFERENCES

1. Rothe, D.E.: Electron-Beam Studies of Viscous Flow in Supersonic Nozzles. AIAA J., vol. 9, no. 5, May 1971, pp. 804-811.

2. Rae, W.J.: Some Numerical Results on Viscous Low-Density Nozzle Flows in the Slender-Channel Approximation. AIAA J., vol. 9, no. 5, May 1971, pp. 811-820.

3. Driscoll, R.J.: Study of the Boundary Layers in Chemical Laser Nozzles. AIAA J., vol. 14, no. 11, Nov. 1976, pp. 1571-1577.

4. Whitfield, D.L.; Lewis, J.W.L.; and Williams, W.D.: Measurements in the Near Field of Supersonic Nozzles for Chemical Laser Systems. AIAA J., vol. 12, no. 6, June 1974, pp. 870-872.

5. Greenberg, R.A., et al.: Rapid Expansion Nozzles for Gas Dynamic Lasers. AIAA J., vol. 10, no. 11, Nov. 1972, pp. 1494-1498.

6. Whitfield, D.L.; and Lewis, C.H.: Boundary-Layer Analysis of Low-Density Nozzles, Including Displacement, Slip, and Transverse Curvature. J. Spacecraft Rockets, vol. 7, no. 4, Apr. 1970, pp. 462-468.

7. Whitfield, D.L.: Theoretical and Experimental Investigation of Boundary Layers in Low Density Hypersonic Axisymmetric Nozzles. AEDC-TR-68-193, Sept. 1968. (Avail. NTIS, AD-674597.)

8. Murch, C.K., et al.: Low-Thrust Nozzle Performance. AIAA Paper 68-91, Jan. 1968.

9. Brophy, J.R.; Pivirotto, T.J.; and King, D.Q.: Investigation of Arcjet Nozzle Performance. AIAA Paper 85-2016, Sept. 1985.

10. Grisnik, S.P.; Smith, T.A.; and Saltz, L.E.: Experimental Study of Low Reynolds Number Nozzles. AIAA Paper 87-0992, May 1987. (NASA TM-89858.)

11. Edwards, I.; and Jansson, R.E.W.: Gasdynamics of Resistojets. J. British Interplanetary Soc., vol. 24, 1971, pp. 729-742.

12. Edwards, I.; and Jansson, R.E.W.: Energy Loss Processes in Resistojet Nozzle Flows. AIAA Paper 72-455, Apr. 1972.

13. Jansson, R.E.W.; and Edwards, I: Theoretical Performance of Ammonia' Hydrogen and Biowaste Resistojets. J. British Interplanetary Soc., vol. 27, no. 6, June 1974, pp. 433-442.

14. Yoshida, R.Y.; Halbach, C.R.; and Hill, C.S.: Life Test Summary and High-Vacuum of 10-mlb Resistojets. J. Spacecraft Rockets, vol. 8, no. 4, Apr. 1971, pp. 414-416.

15. Manzella, D.H., et al.: Effects of Ambient Pressure on the Performance of a Resistojet. AIAA Paper 87-991, May 1987.

16. Sovey, J.S., et al.: Vacuum Chamber Pressure Effects on Thrust Measurements of Low Reynolds Number Nozzles. NASA TM-86955, 1985.

17. Back, L.H.; Massier, P.F.; and Gier, H.L.: Comparison of Measured and Predicted Flows Through Conical Supersonic Nozzles, with Emphasis on the Transonic Region. AIAA J., vol. 3, no. 9, Sept. 1965, pp. 1606-1614.

18. Back, L.H.; Cuffel, R.F.; and Massier, P.F.: Influence of Contraction Section Shape and Inlet Flow Direction on Supersonic Nozzle Flow and Performance. J. Spacecraft Rockets, vol. 9, no. 6, June 1972, pp. 420-427.

19. Campbell, C.E.; and Farley, J.M.: Performance of Several Conical Convergent-Divergent Rocket-Type Exhaust Nozzles. NASA TN D-467, 1960.

20. Back, L.H.; and Cuffel, R.F.: Flow Coefficients for Supersonic Nozzles with Comparatively Small Radius of Curvature Throats. J. Spacecraft Rockets, vol. 8, no. 2, Feb. 1971, pp. 196-198.

21. Cuffel, R.F.; Back, L.H.; and Massier, P.F.: Transonic Flowfield in a Supersonic Nozzle with Small Throat Radius of Curvature. AIAA J., vol. 7, no. 7, July 1969, pp. 1364-1366.

22. Hopkins, D.F.; and Hill, D.E.: Effect of Small Radius of Curvature on Transonic Flow in Axisymmetric Nozzles. AIAA J., vol. 4, no. 8, Aug. 1966, pp. 1337-1343.

23. Kuluva, N.M.; and Hosack, G.A.: Supersonic Nozzle Discharge Coefficients at Low Reynolds Numbers. AIAA J., vol. 9, no. 9, Sept. 1971, pp. 1876-1879.

24. Milligan, M.W.: Nozzle Characteristics in the Transition Regime between Continuum and Free Molecular Flow. AIAA J., vol. 2, no. 6, June 1964, pp. 1088-1092.

25. Rae, W.J.: Study of Low-Density Nozzle Flows, with Application to Microthrust Rockets. NASA CR-107299, 1969.

26. Williams, J.C., III: Viscous Compressible and Incompressible Flow in Slender Channels. AIAA J., vol. 1, no. 1, Jan. 1963, pp. 186-195.

27. Mitra, N.K.; and Fiebig, M.: Supersonic Nozzle Flowfields: a Comparison of Fully Viscous and Navier-Stokes Solutions. Recent Developments in Theoretical and Experimental Fluid Mechanics, U. Muller, K.G. Roesner, and B. Schmidt, eds., Springer Verlag, 1976, pp. 157-165.

28. Rao, G.V.R.: Exhaust Nozzle Contour for Optimum Thrust. Jet Propulsion, vol. 28, no. 6, June 1958, pp. 377-382.

29. Kallis, J.M.; Goodman, M.; and Halbach, C.R.: Viscous Effects on Biowaste Resistojet Nozzle Performance. J. Spacecraft Rockets, vol. 9, no. 12, Dec. 1972, pp. 869-875.

TABLE I. - DEFINITION OF NOZZLE GEOMETRY

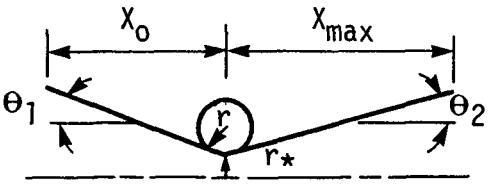

θ_1	ϵ	θ_2	r/r_*	X_o	X_{max}
45	50	15	2.67	-5	11.5
	150	15			20.9
	50	20			8.6
	150	20			15.5
	50	25			6.8
	150	25			12.2

TABLE II. - NUMERICAL METHOD RESULTS FOR NITROGEN

Run number	ϵ	θ_2	B	A_{given}	A_{code}	M*	M_e	C_T
20	50	15	999	0.1139	0.1160	0.962	3.42	1.352
21	50		3600	.1269	.1239	1.002	4.17	1.524
22	50		8823	.1289	-----	-----	----	----
23	150		923	.1257	.1168	1.026	4.65	1.294
24	150		3534	.1287	.1241	1.020	5.07	1.537
25	150		8914	.1281	-----	-----	----	-----
26	50	20	890	.1277	.1159	.994	3.74	1.364
27	50		3536	.1286	.1241	1.020	4.05	1.534
28	50		8880	.1280	-----	----	----	-----
29	150		944	.1204	.1159	.976	4.30	1.378
30	150		3569	.1280	.1241	1.017	4.90	1.556
31	150		9029	.1267	-----	-----	----	-----
32	50	25	918	.1238	.1159	.984	3.75	1.386
33	50		3542	.1283	.1241	1.019	4.06	1.543
34	50		8949	.1278	-----	-----	----	-----
35	150		923	.1232	.1168	1.026	4.59	1.400
36	150		3560	.1277	.1241	1.018	4.96	1.569
37	150		8941	.1279	-----	-----	----	-----

TABLE III. - NUMERICAL METHOD RESULTS FOR HYDROGEN

Run number	ϵ	θ_2	B	A_{given}	A_{code}	M*	M_e	C_T
1	50	15	561	0.1154	0.1120	0.983	3.91	1.238
2	50	↓	3746	.1226	.1226	.932	3.20	1.469
3	50	↓	6556	.1246	-----	-----	-----	-----
4	150	↓	531	.1232	.1168	1.192	1.73	1.132
5	150	↓	3760	.1212	.1241	1.002	4.99	1.540
6	150	↓	6850	.1234	-----	-----	-----	-----
7	50	20	548	.1188	.1168	1.178	3.81	1.328
8	50	↓	3724	.1225	.1225	.929	2.54	1.408
9	50	↓	6801	.1245	-----	-----	-----	-----
10	150	↓	587	.1109	.1109	.933	4.21	1.274
11	150	↓	3788	.1203	.1203	.865	4.10	1.496
12	150	↓	6919	.1223	-----	-----	-----	-----
13	50	25	571	.1141	.1120	.977	3.65	1.307
14	50	↓	3761	.1215	.1215	.897	3.33	1.424
15	50	↓	6853	.1234	-----	-----	-----	-----
16	150	↓	543	.1199	.1168	1.182	4.41	1.338
17	150	↓	3790	.1204	.1204	.868	3.92	1.496
18	150	↓	6896	.1224	-----	-----	-----	-----

TABLE IV. - COMPARISON OF NITROGEN EXPERIMENTAL AND NUMERICAL PERFORMANCE RESULTS

θ_2	ϵ	Re	C_T experiment	C_T numerical	Percent difference
15	50	460	1.29	1.341	+7.6
15	50	1845	1.25	1.524	+3.1
15	150	460	1.25	1.294	+3.5
15	150	1847	1.50	1.537	+3.4
20	50	458	1.40	1.365	-2.2
20	50	1830	1.51	1.534	+1.6
20	150	460	1.33	1.378	+3.9
20	150	1848	1.52	1.556	+2.4
25	50	458	1.34	1.384	+2.9
25	50	1848	1.50	1.556	+3.0
25	150	462	1.38	1.399	+1.3
25	150	1848	1.53	1.569	+2.5

TABLE V. - COMPARISON OF HYDROGEN EXPERIMENTAL AND NUMERICAL PERFORMANCE RESULTS

θ_2	ε	Re	C_T experiment	C_T numerical	Percent difference
15	50	263	1.15	1.238	+7.7
15	50	1836	1.47	1.469	+0.2
15	150	265	1.23	1.132	-8.0
15	150	1836	1.47	1.540	+4.8
20	50	265	1.11	1.328	+20
20	50	1852	1.46	1.408	+3.3
20	150	262	1.11	1.276	+14
20	150	1838	1.46	1.496	+2.0
25	50	260	1.16	1.307	+12
25	50	1834	1.46	1.474	+1.1
25	150	261	1.26	1.338	+5.9
25	150	1829	1.46	1.496	+2.3

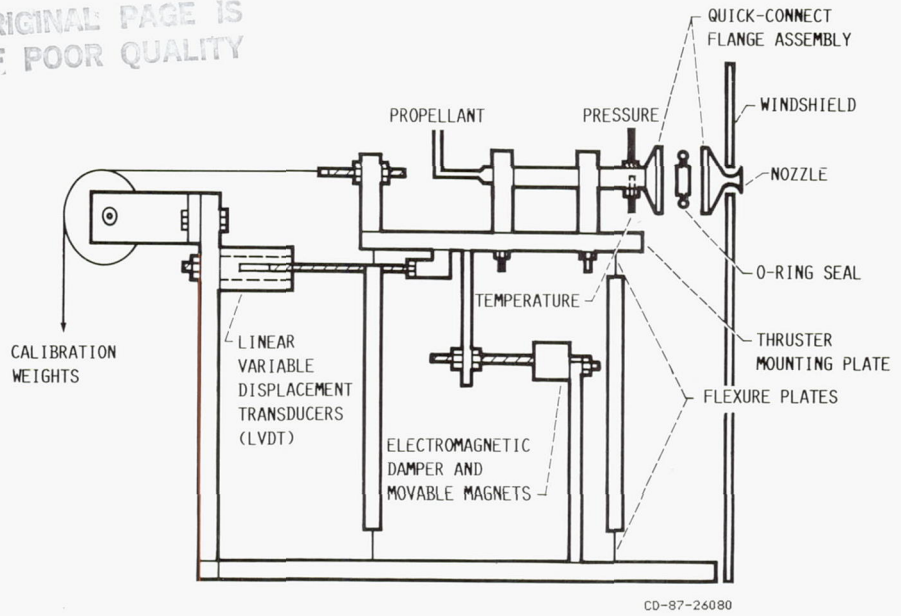

FIGURE 1. - SCHEMATIC OF NOZZLE ASSEMBLY AND THRUST STAND.

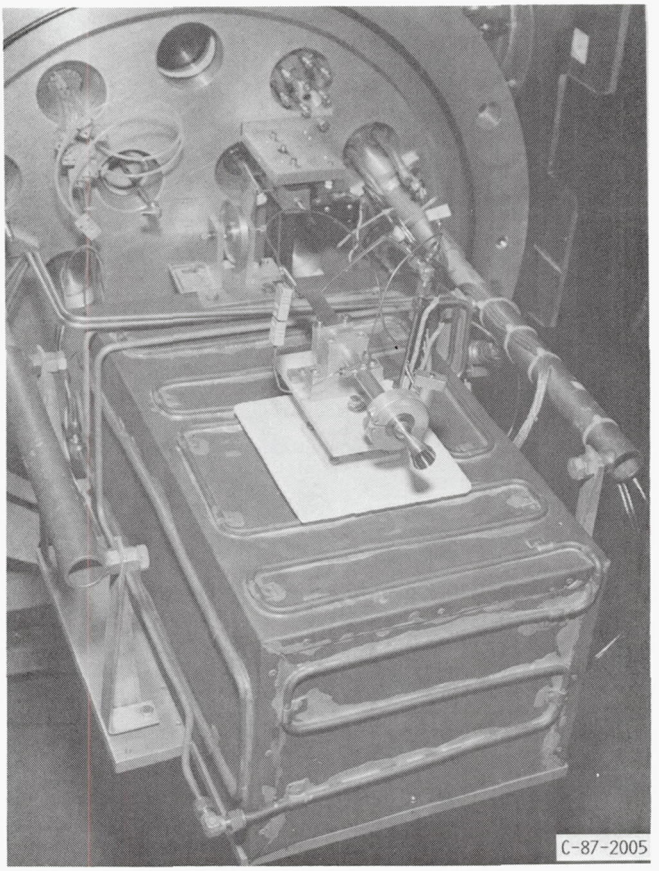

FIGURE 2. - NOZZLE ASSEMBLY ON THRUST STAND.

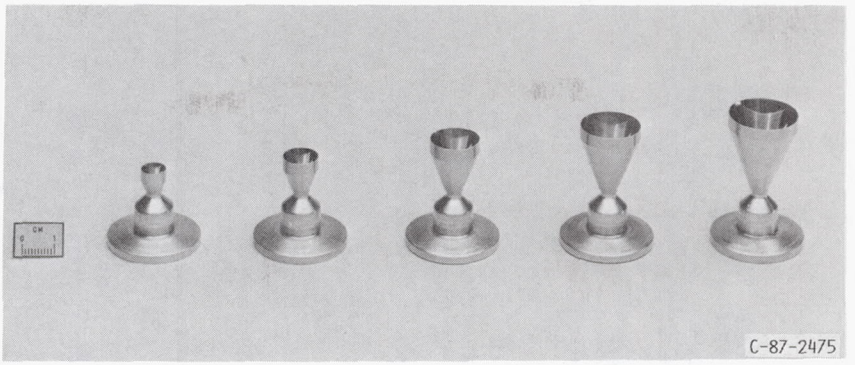

FIGURE 3. - DIFFERENT AREA RATIO 20° CONICAL NOZZLES WITH FLANGE.

TABLE OF DIMENSIONS, MM					
PART NUMBER	θ	IDE	ε^*	L_1	L_2
6152	15°	10.79	50	17.27	25.91
6153		15.26	100	25.60	34.24
6154		18.64	150	31.98	40.64
6155		21.53	200	37.36	46.00
6201	20°	7.66	25	8.38	17.02
6202		10.77	50	12.70	21.34
6203		15.14	99	18.85	27.48
6204		18.65	150	23.55	32.18
6205		21.56	200	27.50	36.14
6251	25°	7.69	25	6.53	15.16
6252		10.78	50	9.93	18.54
6253		15.14	99	14.70	23.34
6254		18.67	150	18.39	27.03
6255		21.50	199	21.49	30.12

*ε = AREA RATIO.

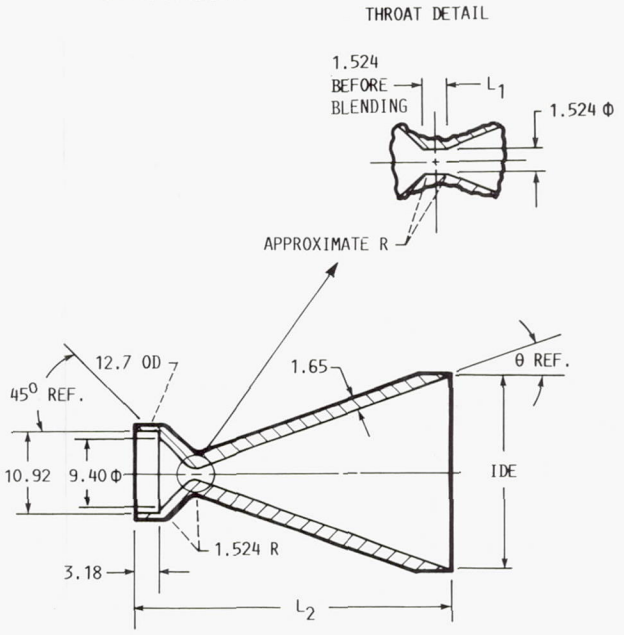

FIGURE 4. - CONICAL NOZZLE DESIGN. (ALL DIMENSIONS ARE IN MILLIMETERS.)

FIGURE 5. - DIFFERENT AREA RATIO BELL NOZZLES WITH FLANGES.

TABLE OF DIMENSIONS, MM				
PART NUMBER	IDE	ε^*	L_1	L_2
8.61	7.645	26	10.16	18.80
8.62	10.87	52	16.40	25.04
8.63	15.24	104	26.34	34.96
8.64	18.62	154	34.70	43.33
8.65	21.54	205	42.16	50.80

*ε = AREA RATIO.

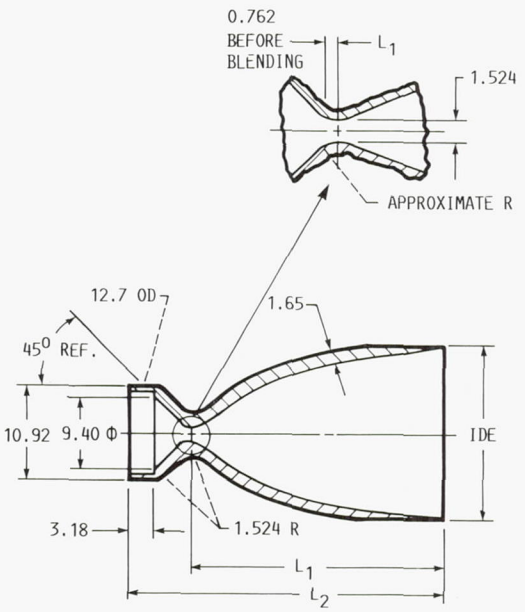

FIGURE 6. - BELL NOZZLE DESIGN. (ALL DIMENSIONS ARE IN MILLIMETERS.)

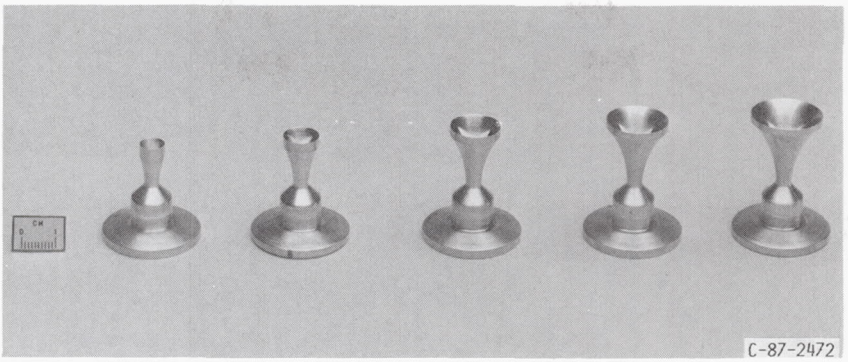

FIGURE 7. - DIFFERENT AREA RATIO TRUMPET NOZZLES WITH FLANGES.

TABLE OF DIMENSIONS, MM				
PART NUMBER	DIA	L_1	L_2	ε^*
H425	7.643	9.14	17.02	26
H450	10.78	10.95	18.82	51
H4100	15.24	12.73	20.60	103
H4150	18.66	13.69	21.56	155
H4200	21.58	14.32	22.20	207

*ε = AREA RATIO.

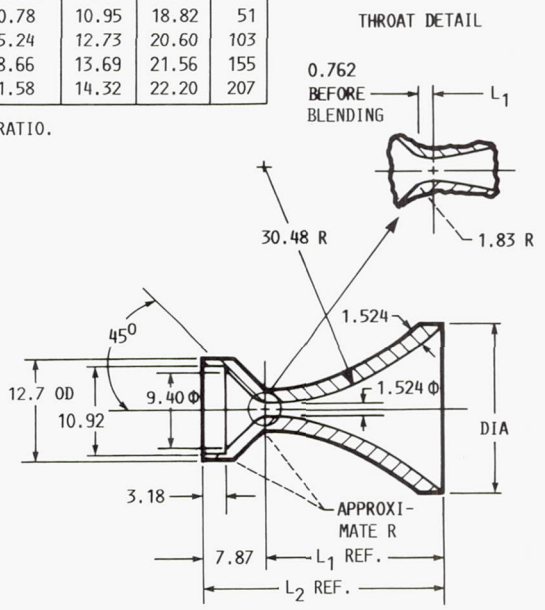

FIGURE 8. - TRUMPET NOZZLE DESIGN. (ALL DIMENSIONS ARE IN MILLIMETERS.)

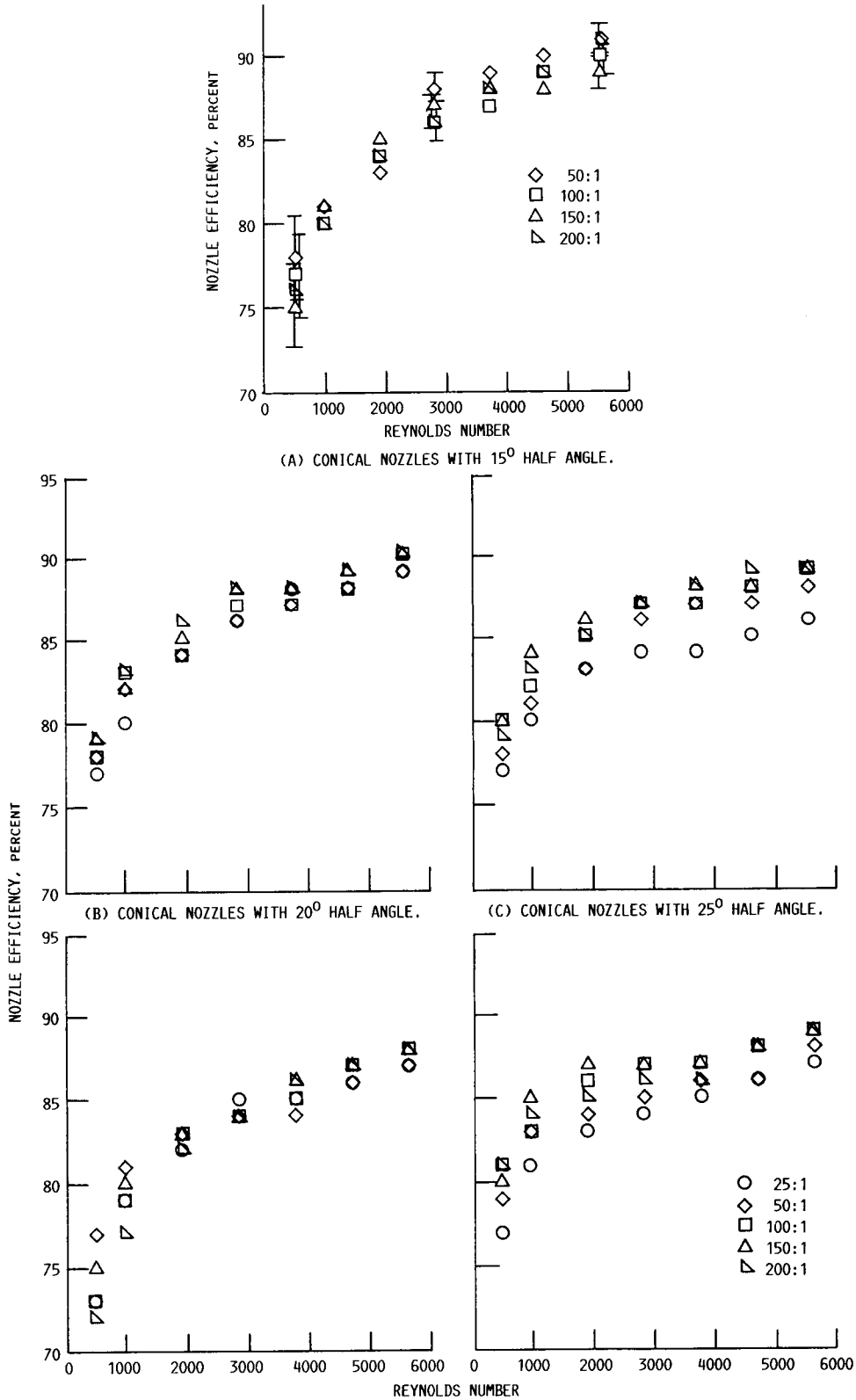

FIGURE 9. - NOZZLE EFFICIENY VARIATION WITH AREA RATIO, UNHEATED NITROGEN.

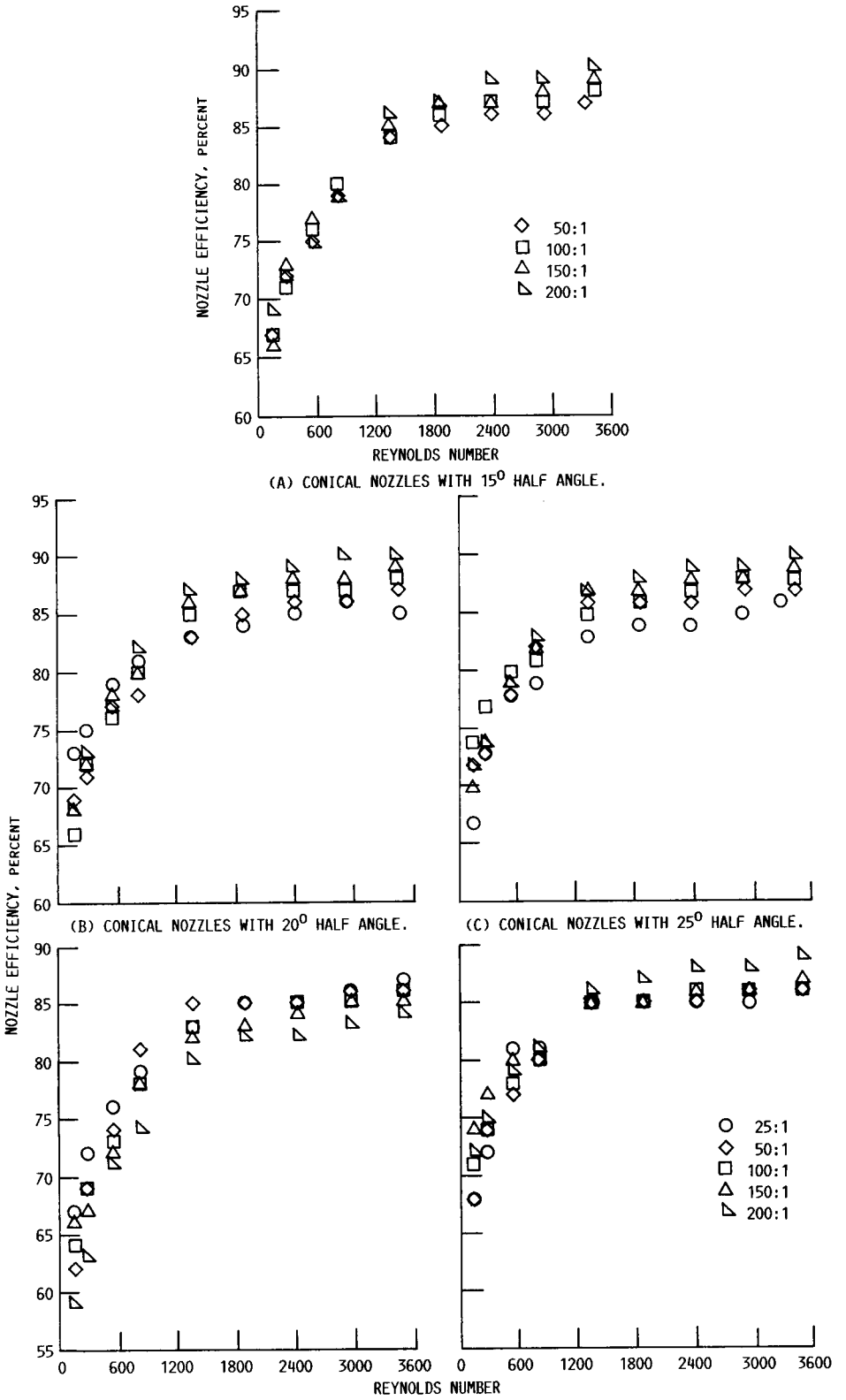

(A) CONICAL NOZZLES WITH 15^{0} HALF ANGLE.

(B) CONICAL NOZZLES WITH 20^{0} HALF ANGLE.

(C) CONICAL NOZZLES WITH 25^{0} HALF ANGLE.

(D) BELL NOZZLES.

(E) TRUMPET NOZZLES.

FIGURE 10. - NOZZLE EFFICIENCY VARIATION WITH AREA RATIO, UNHEATED HYDROGEN.

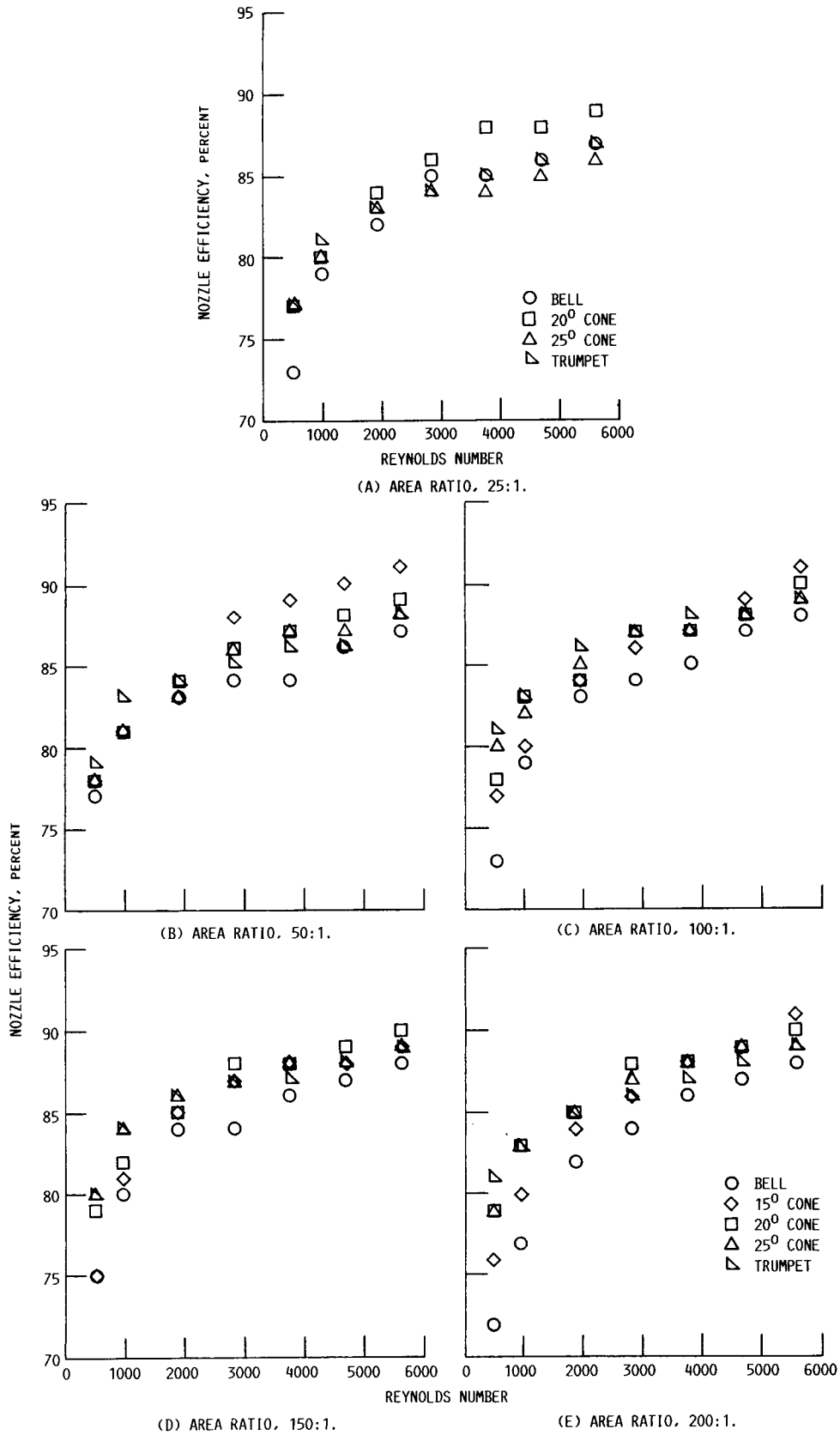

(A) AREA RATIO, 25:1.

(B) AREA RATIO, 50:1.

(C) AREA RATIO, 100:1.

(D) AREA RATIO, 150:1.

(E) AREA RATIO, 200:1.

FIGURE 11. - NOZZLE EFFICIENCY FOR VARIOUS CONTOURS WITH UNHEATED NITROGEN.

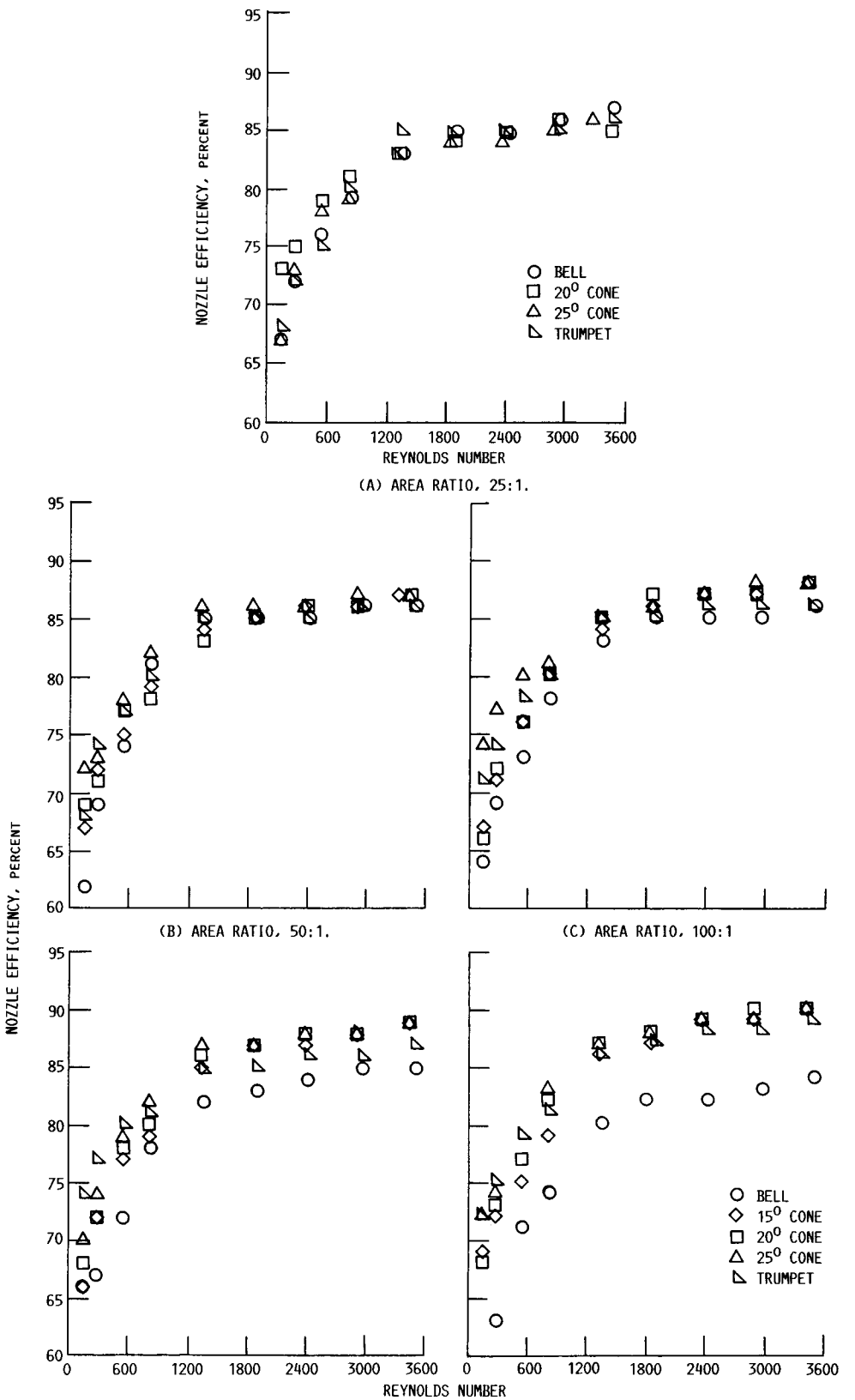

FIGURE 12. - NOZZLE EFFICIENCY FOR VARIOUS CONTOURS WITH UNHEATED HYDROGEN.

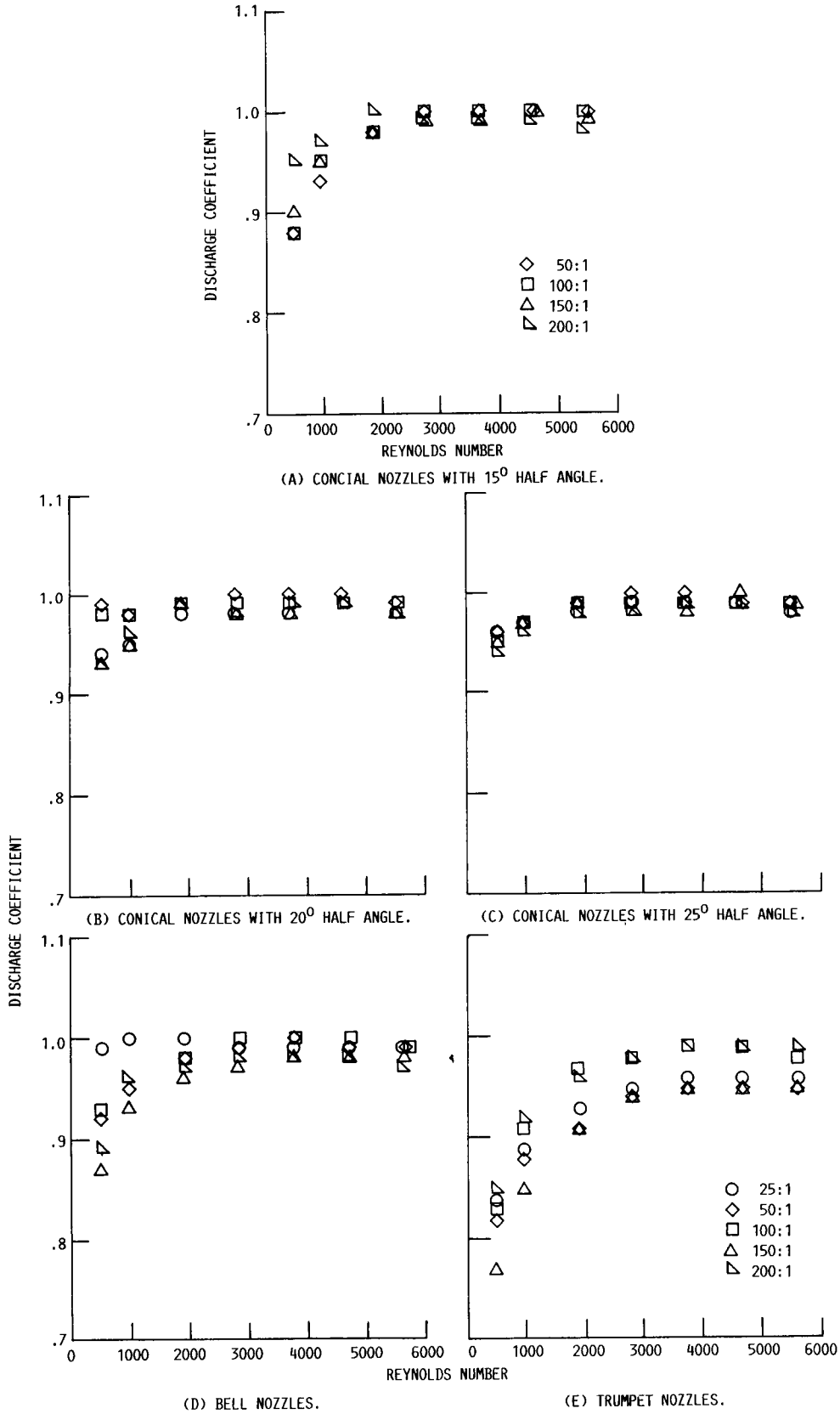

(A) CONCIAL NOZZLES WITH 15^{0} HALF ANGLE.

(B) CONICAL NOZZLES WITH 20^{0} HALF ANGLE.

(C) CONICAL NOZZLES WITH 25^{0} HALF ANGLE.

(D) BELL NOZZLES.

(E) TRUMPET NOZZLES.

FIGURE 13. - DISCHARGE COEFFICIENT VARIATION WITH AREA RATIO, UNHEATED NITROGEN.

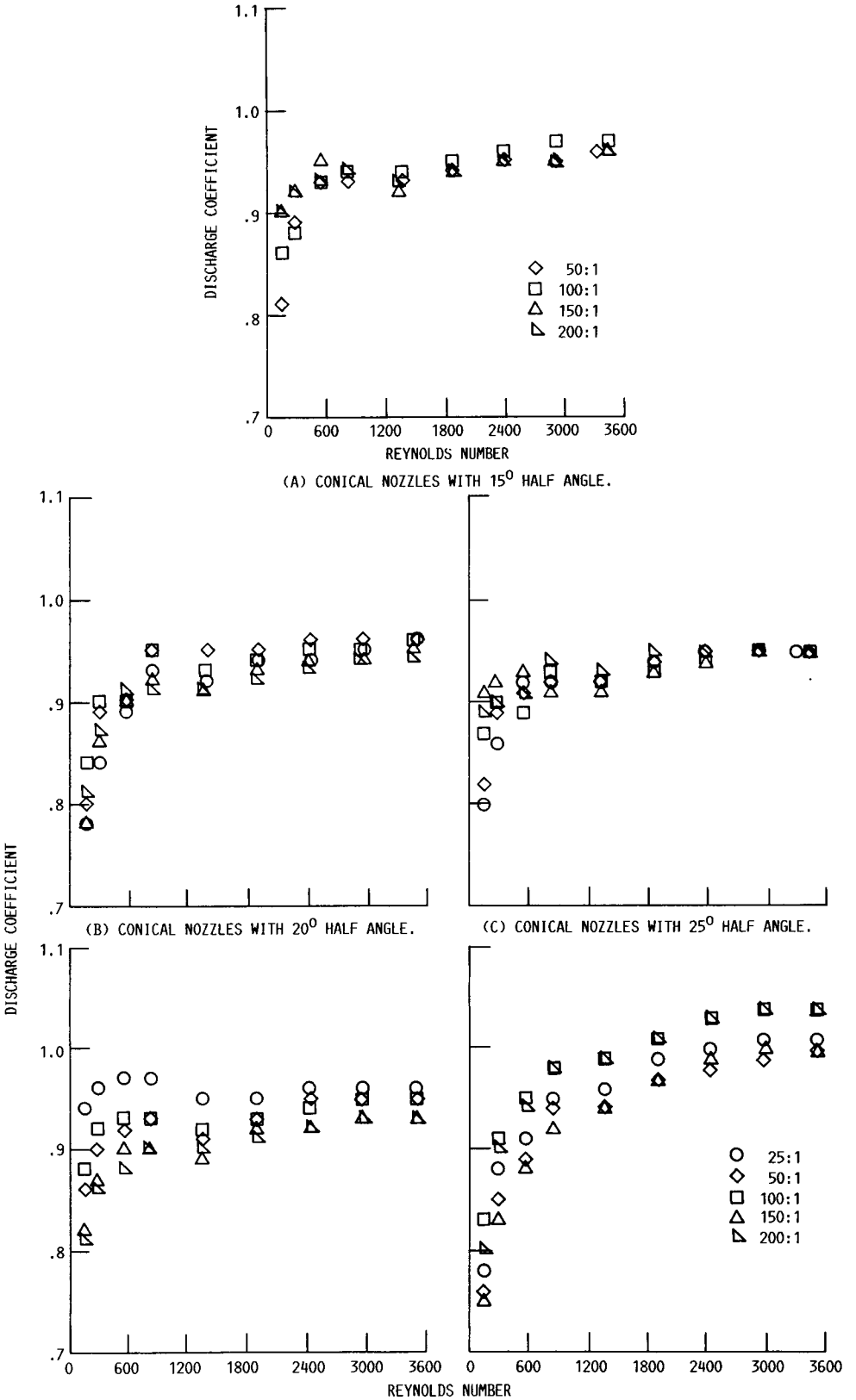

(A) CONICAL NOZZLES WITH 15^{0} HALF ANGLE.

(B) CONICAL NOZZLES WITH 20^{0} HALF ANGLE.

(C) CONICAL NOZZLES WITH 25^{0} HALF ANGLE.

(D) BELL NOZZLES.

(E) TRUMPET NOZZLES.

FIGURE 14. - DISCHARGE COEFFICIENT VARIATION WITH AREA RATIO, UNHEATED HYDROGEN.

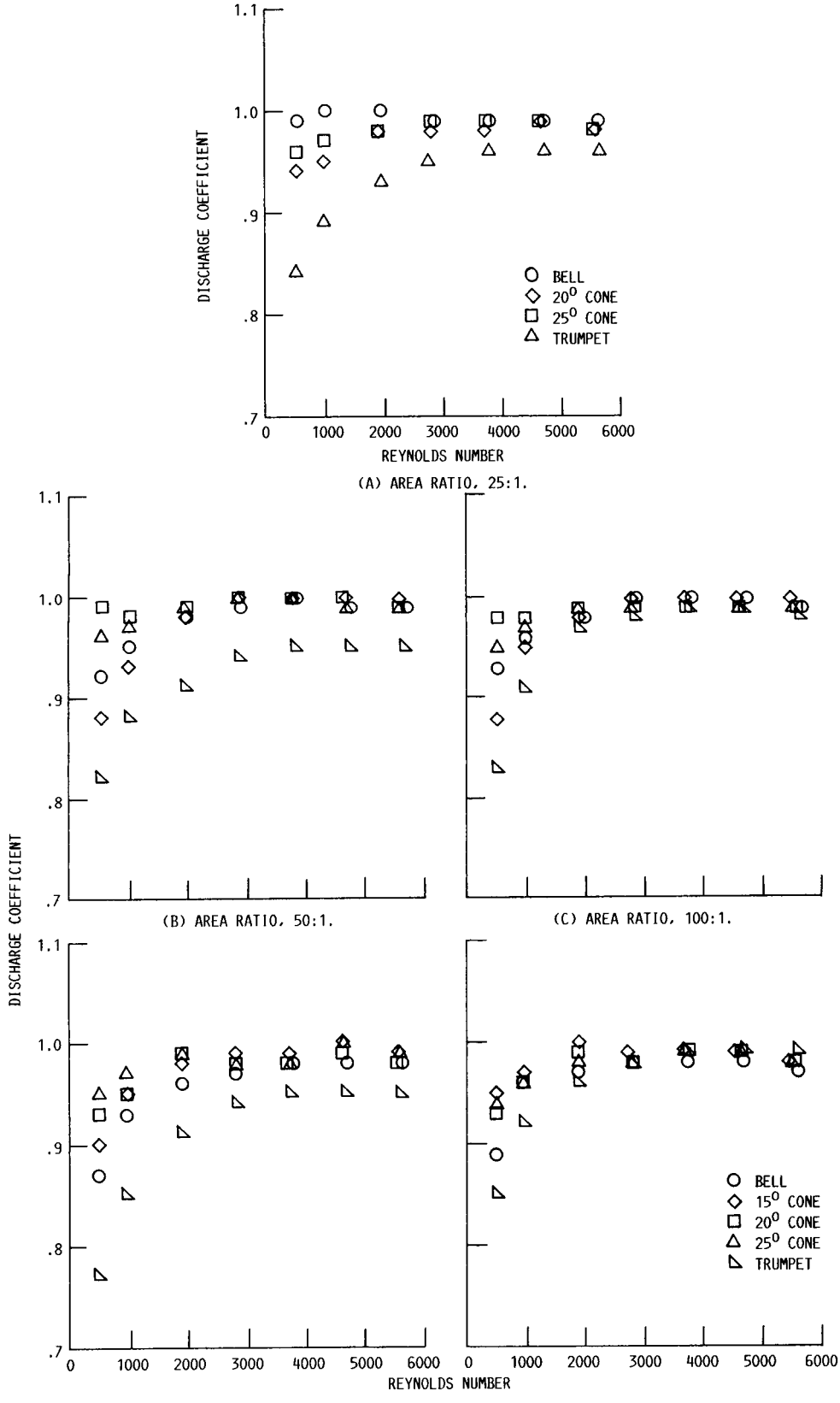

(A) AREA RATIO, 25:1.

(B) AREA RATIO, 50:1.

(C) AREA RATIO, 100:1.

(D) AREA RATIO, 150:1.

(E) AREA RATIO, 200:1.

FIGURE 15. - DISCHARGE COEFFICIENT FOR VARIOUS CONTOURS WITH UNHEATED NITROGEN.

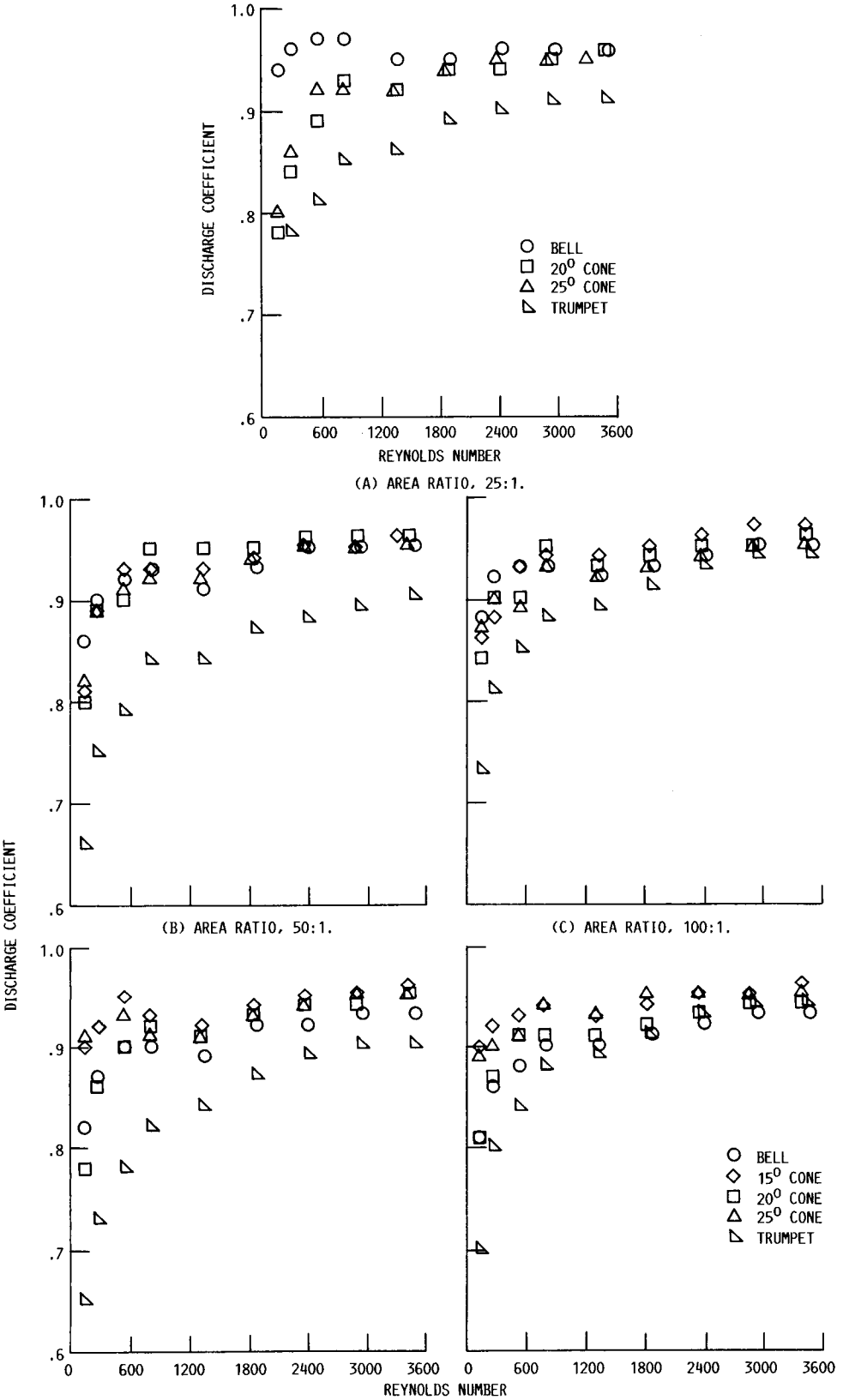

(A) AREA RATIO, 25:1.

(B) AREA RATIO, 50:1.

(C) AREA RATIO, 100:1.

(D) AREA RATIO, 150:1.

(E) AREA RATIO, 200:1.

FIGURE 16. - DISCHARGE COEFFICIENT FOR VARIOUS CONTOURS WITH UNHEATED HYDROGEN.

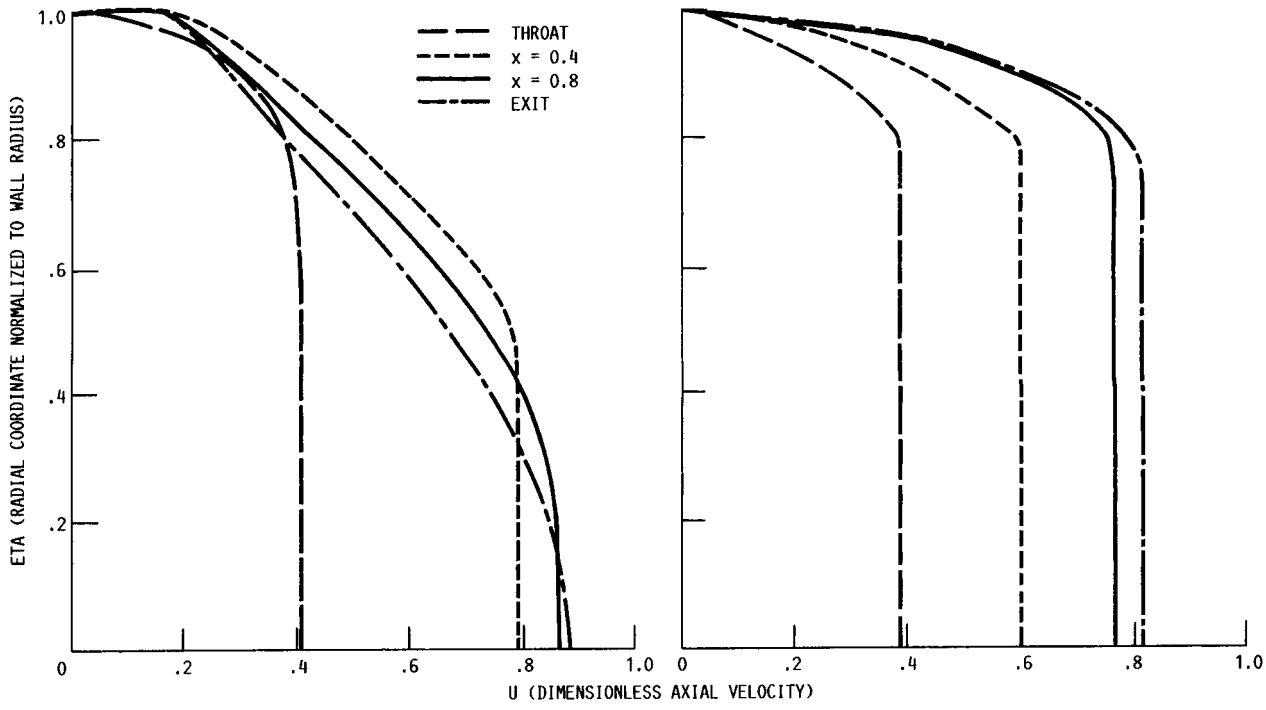

(A) REYNOLDS NUMBER OF 260.

(B) REYNOLDS NUMBER OF 1850.

FIGURE 17. - VELOCITY PROFILES AT VARIOUS AXIAL LOCATIONS FOR THE 15^{o} CONICAL WITH AREA RATIO 50:1.

NASA
National Aeronautics and Space Administration

Report Documentation Page

1. Report No.	2. Government Accession No.	3. Recipient's Catalog No.
NASA TM-100130		

4. Title and Subtitle	5. Report Date
Low Reynolds Number Nozzle Flow Study	July 1987
	6. Performing Organization Code: 506-42-31

7. Author(s)	8. Performing Organization Report No.
Margaret V. Whalen	E-3679
	10. Work Unit No.

9. Performing Organization Name and Address	11. Contract or Grant No.
National Aeronautics and Space Administration Lewis Research Center Cleveland, Ohio 44135	13. Type of Report and Period Covered: Technical Memorandum
12. Sponsoring Agency Name and Address	14. Sponsoring Agency Code
National Aeronautics and Space Administration Washington, D.C. 20546	

15. Supplementary Notes

This report was a thesis submitted in partial fulfillment of the requirements for the Master of Science Degree in Mechanical Engineering to The University of Toledo, Toledo, Ohio.

16. Abstract

An experimental study of low Reynolds number nozzle flow was performed. A brief comparison was made between some of the experimental performance data and performance predicted by a viscous flow code. The performance of 15°, 20°, and 25° conical nozzles, bell nozzles, and trumpet nozzles was evaluated with unheated nitrogen and hydrogen. The numerical analysis was applied to the conical nozzles only, using an existing viscous flow code that was based on a slender-channel approximation. Although the trumpet and 25° conical nozzles had slightly better performance at lower Reynolds numbers, it is unclear which nozzle is superior as all fell within the experimental error band. The numerical results were found to agree with experimental results for nitrogen and for some of the hydrogen data. Some code modification is recommended to improve confidence in the performance prediction.

17. Key Words (Suggested by Author(s))	18. Distribution Statement
Nozzles; Low Reynolds number flow; Resistojet nozzles; Arcjet nozzles; Rae nozzle code	Unclassified - unlimited STAR Category 20

19. Security Classif. (of this report)	20. Security Classif. (of this page)	21. No of pages	22. Price*
Unclassified	Unclassified	43	A03

*For sale by the National Technical Information Service, Springfield, Virginia 22161